

## RESEARCH ARTICLE

10.1002/2018JD028336

## Special Section:

Winter INvestigation of  
Transport, Emissions and  
Reactivity (WINTER)

## Key Points:

- Aircraft measurements over the eastern United States provide the largest number of  $\text{N}_2\text{O}_5$  uptake coefficient  $\gamma(\text{N}_2\text{O}_5)$  determinations during winter
- Despite a large range and variability, several  $\gamma(\text{N}_2\text{O}_5)$  dependencies are statistically significant, particularly with aerosol liquid water
- Standard  $\gamma(\text{N}_2\text{O}_5)$  parameterizations do not capture the variability but several, including an empirical form derived here, capture the median

## Supporting Information:

- Supporting Information S1

## Correspondence to:

S. S. Brown,  
steven.s.brown@noaa.gov

## Citation:

McDuffie, E. E., Fibiger, D. L., Dubé, W. P., Lopez-Hilfiker, F., Lee, B. H., Thornton, J. A., et al. (2018). Heterogeneous  $\text{N}_2\text{O}_5$  uptake during winter: Aircraft measurements during the 2015 WINTER campaign and critical evaluation of current parameterizations. *Journal of Geophysical Research: Atmospheres*, 123, 4345–4372. <https://doi.org/10.1002/2018JD028336>





















Received 15 JAN 2018

Accepted 22 MAR 2018

Accepted article online 30 MAR 2018

Published online 21 APR 2018

Heterogeneous  $\text{N}_2\text{O}_5$  Uptake During Winter: Aircraft Measurements During the 2015 WINTER Campaign and Critical Evaluation of Current Parameterizations

Erin E. McDuffie<sup>1,2,3</sup> , Dorothy L. Fibiger<sup>1,2</sup> , William P. Dubé<sup>1,2</sup>, Felipe Lopez-Hilfiker<sup>4</sup>, Ben H. Lee<sup>4</sup> , Joel A. Thornton<sup>4</sup> , Viral Shah<sup>4</sup> , Lyatt Jaeglé<sup>4</sup> , Hongyu Guo<sup>5</sup> , Rodney J. Weber<sup>5</sup> , J. Michael Reeves<sup>6</sup>, Andrew J. Weinheimer<sup>7</sup> , Jason C. Schroder<sup>2,3</sup> , Pedro Campuzano-Jost<sup>2,3</sup> , Jose L. Jimenez<sup>2,3</sup> , Jack E. Dibb<sup>8</sup> , Patrick Veres<sup>1,2</sup> , Carly Ebben<sup>9</sup>, Tamara L. Sparks<sup>9</sup> , Paul J. Wooldridge<sup>9</sup>, Ronald C. Cohen<sup>9</sup> , Rebecca S. Hornbrook<sup>7</sup> , Eric C. Apel<sup>7</sup> , Teresa Campos<sup>7</sup>, Samuel R. Hall<sup>7</sup> , Kirk Ullmann<sup>7</sup>, and Steven S. Brown<sup>1,3</sup> 
<sup>1</sup>Chemical Sciences Division, Earth System Research Laboratory, NOAA, Boulder, CO, USA, <sup>2</sup>Cooperative Institute for Research in Environmental Sciences, University of Colorado Boulder, Boulder, CO, USA, <sup>3</sup>Department of Chemistry, University of Colorado Boulder, Boulder, CO, USA, <sup>4</sup>Department of Atmospheric Sciences, University of Washington, Seattle, WA, USA, <sup>5</sup>Earth and Atmospheric Sciences Department, Georgia Institute of Technology, Atlanta, GA, USA, <sup>6</sup>Earth Observing Laboratory, NCAR, Boulder, CO, USA, <sup>7</sup>Atmospheric Chemistry Observations & Modeling Laboratory, NCAR, Boulder, CO, USA, <sup>8</sup>Institute for the Study of Earth, Oceans, and Space, University of New Hampshire, Durham, NH, USA, <sup>9</sup>Department of Chemistry, University of California Berkeley, Berkeley, CA, USA

**Abstract** Nocturnal dinitrogen pentoxide ( $\text{N}_2\text{O}_5$ ) heterogeneous chemistry impacts regional air quality and the distribution and lifetime of tropospheric oxidants. Formed from the oxidation of nitrogen oxides,  $\text{N}_2\text{O}_5$  is heterogeneously lost to aerosol with a highly variable reaction probability,  $\gamma(\text{N}_2\text{O}_5)$ , dependent on aerosol composition and ambient conditions. Reaction products include soluble nitrate ( $\text{HNO}_3$  or  $\text{NO}_3^-$ ) and nitryl chloride ( $\text{ClNO}_2$ ). We report the first-ever derivations of  $\gamma(\text{N}_2\text{O}_5)$  from ambient wintertime aircraft measurements in the critically important nocturnal residual boundary layer. Box modeling of the 2015 Wintertime INvestigation of Transport, Emissions, and Reactivity (WINTER) campaign over the eastern United States derived 2,876 individual  $\gamma(\text{N}_2\text{O}_5)$  values with a median value of 0.0143 and range of  $2 \times 10^{-5}$  to 0.1751. WINTER  $\gamma(\text{N}_2\text{O}_5)$  values exhibited the strongest correlation with aerosol water content, but weak correlations with other variables, such as aerosol nitrate and organics, suggesting a complex, nonlinear dependence on multiple factors, or an additional dependence on a nonobserved factor. This factor may be related to aerosol phase, morphology (i.e., core shell), or mixing state, none of which are commonly measured during aircraft field studies. Despite general agreement with previous laboratory observations, comparison of WINTER data with 14 literature parameterizations (used to predict  $\gamma(\text{N}_2\text{O}_5)$  in chemical transport models) confirms that none of the current methods reproduce the full range of  $\gamma(\text{N}_2\text{O}_5)$  values. Nine reproduce the WINTER median within a factor of 2. Presented here is the first field-based, empirical parameterization of  $\gamma(\text{N}_2\text{O}_5)$ , fit to WINTER data, based on the functional form of previous parameterizations.

## 1. Introduction

The chemical formation and nocturnal fate of tropospheric  $\text{N}_2\text{O}_5$  strongly influences the availability and distribution of tropospheric oxidants, such as ozone ( $\text{O}_3$ ), the hydroxyl radical ( $\text{OH}$ ), and nitrogen oxides ( $\text{NO}_x = \text{NO} + \text{NO}_2$ ) (Dentener & Crutzen, 1993; Macintyre & Evans, 2010; Tie et al., 2001). This chemistry is also vitally important to ammonium nitrate particle formation under cold conditions or in regions of large  $\text{NH}_3$  emissions (Baasandorj et al., 2017; Pusede et al., 2016; Riemer et al., 2003) and has implications for regional air quality control strategies due to negative health impacts of particulate matter  $< 2.5 \mu\text{m}$  in diameter (Dockery et al., 1993). Formed from the oxidation of  $\text{NO}_x$ ,  $\text{N}_2\text{O}_5$  exists in thermochemical equilibrium with the nitrate radical ( $\text{NO}_3$ ), as shown by the scheme in Figure 1. The short lifetime of  $\text{NO}_3$  against photolysis and reaction with photochemically-generated  $\text{NO}$  prevents buildup of appreciable  $\text{N}_2\text{O}_5$  mixing ratios ( $> 10 \text{ pptv}$ ) during the day (e.g., Brown et al., 2005). Reaction of  $\text{NO}_3$  with  $\text{NO}$  near  $\text{NO}_x$  emission sources will also suppress  $\text{N}_2\text{O}_5$  production at night near the surface. As a result of boundary layer dynamics that

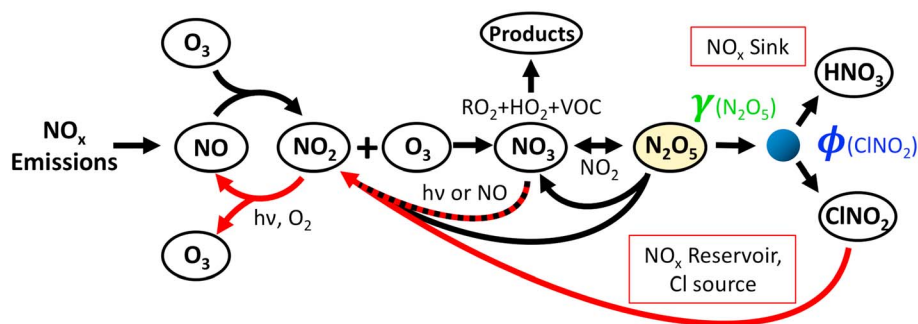


**Figure 1.** Schematic of the  $\text{N}_2\text{O}_5$  chemical system. Black arrows indicate reactions that do not require sunlight; red arrows show photochemical reactions.

decouple the nocturnal boundary layer (NBL) from the residual layer (RL) (Stull, 1988),  $\text{N}_2\text{O}_5$  formed at night near urban areas in the RL will therefore either persist (in equilibrium with  $\text{NO}_3$  and  $\text{NO}_2$ ) until sunrise, or be lost heterogeneously through uptake onto aerosol. The uptake coefficient,  $\gamma(\text{N}_2\text{O}_5)$ , is defined as the net probability  $\text{N}_2\text{O}_5$  will be irreversibly taken up onto an aerosol surface upon collision. Collision and successful surface accommodation are followed by diffusion and aqueous reaction with particle water or chloride to form soluble nitrate ( $\text{HNO}_3 + \text{NO}_3^-$ ) and/or nitryl chloride ( $\text{ClNO}_2$ ), the mechanism of which (Figure 2) has been the topic of many previous studies (e.g., Bertram & Thornton, 2009) and is discussed in later sections. Upon sunrise, unreacted  $\text{N}_2\text{O}_5$  will irreversibly, thermally dissociate back to  $\text{NO}_2$  and  $\text{NO}_3$ , where  $\text{NO}_3$  will rapidly photolyze to form a second  $\text{NO}_2$  molecule that can contribute to  $\text{O}_3$  and the formation of  $\text{NO}_x$  the following day (Figure 1). The product branching ratio between  $\text{HNO}_3$  and photolabile  $\text{ClNO}_2$ , represented by  $\phi(\text{ClNO}_2)$ , also has implications for global distributions of oxidants and chlorine radicals (Osthoff et al., 2008; Sarwar et al., 2014; Thornton et al., 2010) and will be the topic of an upcoming analysis. Overall, the pathways in Figure 1 illustrate the potential role of  $\text{N}_2\text{O}_5$  and its uptake efficiency in the regional transport and distribution of  $\text{NO}_x$  and tropospheric oxidants.

The chemical mechanism and aerosol uptake efficiency of  $\text{N}_2\text{O}_5$  have been primarily studied during northern midlatitude, summertime field campaigns (see references below), despite the greater importance of  $\text{N}_2\text{O}_5$  uptake in governing  $\text{NO}_x$  abundance during winter (e.g., Dentener & Crutzen, 1993). As discussed in Wagner et al. (2013), there are three key differences during winter that can impact  $\text{N}_2\text{O}_5$  chemistry including (1) longer nights that allow more time for  $\text{N}_2\text{O}_5$  production/loss, (2) colder temperatures that favor  $\text{N}_2\text{O}_5$  in its equilibrium with  $\text{NO}_3$ , and (3) differences in aerosol composition (Zhang et al., 2007) that could lead to changes in uptake efficiency. Despite these important differences, only three field studies have reported determinations of  $\text{N}_2\text{O}_5$  uptake efficiencies during the winter season (Brown et al., 2016; Wagner et al., 2013; Wild et al., 2016), and none from aircraft, limiting the altitude and spatial diversity of previous observations.

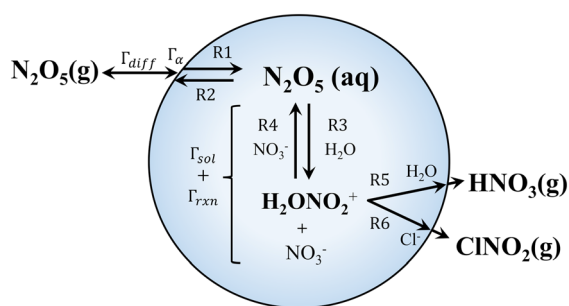


**Figure 2.** Uptake schematic highlighting the relation between the chemical mechanism and resistor model framework in terms of each mechanistic step ((R1)–(R6)) and its associated conductance ( $\Gamma$ ).

The majority of all previous field studies have derived  $\gamma(\text{N}_2\text{O}_5)$  values using the steady state approximation (Brown et al., 2003), which must infer  $\gamma(\text{N}_2\text{O}_5)$  from measurements of aerosol surface area, nitrogen oxides, and  $\text{O}_3$ , and may not be well suited to the cold temperatures and high- $\text{NO}_x$  concentrations encountered during winter in urban areas (Brown et al., 2003). While previous flow tube reactor experiments in ambient air have provided direct measurements of  $\text{N}_2\text{O}_5$  aerosol loss rates (e.g., Bertram, Thornton, & Riedel, 2009), uptake coefficients in these studies must also be calculated from additional aerosol surface area measurements. Additionally challenging is that heterogeneous reactions are complex and driven by many physiochemical, thermodynamic, and kinetic factors that change with ambient conditions and aerosol surface/bulk composition (e.g., Kolb et al., 2002; Pöschl et al., 2007). Previous experiments investigating the mechanism and kinetics

of  $\gamma(\text{N}_2\text{O}_5)$  on laboratory-derived aerosol (Anttila et al., 2006; Bertram & Thornton, 2009; Folkers et al., 2003; Mentel et al., 1999; Mozurkewich & Calvert, 1988; Thornton et al., 2003) show a dependence on several key factors including aerosol surface water availability and composition.

Both laboratory and previous field studies have reported values of  $\gamma(\text{N}_2\text{O}_5)$  between  $\sim 10^{-4}$  and 0.1, a range which Macintyre and Evans (2010) showed can either minimally ( $<3\%$ ) or significantly ( $>15\%$ ) impact the global budgets of  $\text{O}_3$  and OH. This large oxidant sensitivity has led to the development of multiple laboratory-based parameterizations (Anttila et al., 2006; Davis et al., 2008; Evans & Jacob, 2005; Gaston et al., 2014; Riemeier et al., 2003), some in combination with a proposed chemical mechanism (Bertram & Thornton, 2009; Griffiths et al., 2009; Riemeier et al., 2009), to describe  $\gamma(\text{N}_2\text{O}_5)$  as a function of key factors. While one parameterization has successfully predicted field-derived  $\gamma(\text{N}_2\text{O}_5)$  values under certain ambient conditions (Bertram, Thornton, Riedel, Middlebrook, et al., 2009), disagreements largely persist between parameterized and field-derived values (Brown et al., 2009; Chang et al., 2016; Morgan et al., 2015; Phillips et al., 2016; Riedel et al., 2012). Due to the limited number of field studies that have quantified  $\gamma(\text{N}_2\text{O}_5)$ , particularly in winter, these parameterization-field discrepancies could result from comparisons to a relatively small number of data sets, incorrect identification of the factors controlling  $\gamma(\text{N}_2\text{O}_5)$ , or an inaccurate functional dependence on factors already incorporated. The importance of  $\gamma(\text{N}_2\text{O}_5)$  in regulating global concentrations of tropospheric oxidants ( $\text{O}_3$ , OH), combined with its observed orders of magnitude range, highlights the need for a larger database of field-derived  $\gamma(\text{N}_2\text{O}_5)$  values and determination of their dependence on physical and chemical variables.

We present a box model analysis to quantitatively derive  $\gamma(\text{N}_2\text{O}_5)$  under the cold, high- $\text{NO}_x$  conditions encountered during the Wintertime INvestigation of Transport, Emissions, and Reactivity (WINTER) aircraft campaign over the eastern United States in February–March 2015. Box model results are compared to  $\gamma(\text{N}_2\text{O}_5)$  values derived using the steady state approximation to assess this methods applicability to conditions encountered during the WINTER campaign. Observed correlations between box model  $\gamma(\text{N}_2\text{O}_5)$  results and multiple factors of aerosol composition, relative humidity (RH), and temperature are then used in combination with results from a critical evaluation of 14 literature parameterizations to inform the first empirical, field-based parameterization of  $\gamma(\text{N}_2\text{O}_5)$ .

## 2. Methods

### 2.1. WINTER Campaign and Measurements

The WINTER campaign conducted 13 research flights with the National Science Foundation (NSF)/National Center for Atmospheric Research (NCAR) C-130 aircraft over the eastern United States between 3 February and 13 March 2015. Flight tracks in Figure 3a show the geographical distribution of flights conducted during various times of day and night (night defined as solar zenith angle (SZA)  $> 90^\circ$ ) over both continental and marine environments. Aircraft instrumentation included measurements of many species, including reactive nitrogen oxides,  $\text{O}_3$ , and aerosol composition. Several species were measured by duplicate techniques. Instrument details, including accuracy and measurement frequency, are given in Table 1 and described briefly in section S1 of the supporting information.

### 2.2. Iterative Box Model

The iterative box model used in this analysis is based on the description in Wagner et al. (2013), developed to simulate the nocturnal evolution of air sampled at a tall tower in Colorado. Key aspects of the model have been updated for use with WINTER aircraft data and are described briefly below with additional details in supporting information section S2.

#### 2.2.1. Model Description

The first-order loss rate coefficient of  $\text{N}_2\text{O}_5$  ( $k_{\text{N}_2\text{O}_5} [\text{s}^{-1}] = k_{10} + k_{11}$ ) and production rate coefficient of  $\text{ClNO}_2$  ( $k_{\text{ClNO}_2} [\text{s}^{-1}] = k_{11}$ ) were derived for every 10-s period of all WINTER night flights using a zero-dimensional box model, developed to simulate the nocturnal chemical evolution of an air parcel in the RL (assuming constant temperature and RH), from the onset of  $\text{N}_2\text{O}_5$  production (1.3 hr prior to sunset or time of  $\text{NO}_x$  emission, described below) until the time of aircraft measurement. Nighttime data were defined as periods of time with SZA greater than  $90^\circ$ , calculated from aircraft Global Positioning System (GPS) location and time. Model-derived values for  $k_{\text{N}_2\text{O}_5}$  and  $k_{\text{ClNO}_2}$  were then used in equations (E1) and (E2), with aircraft observations of

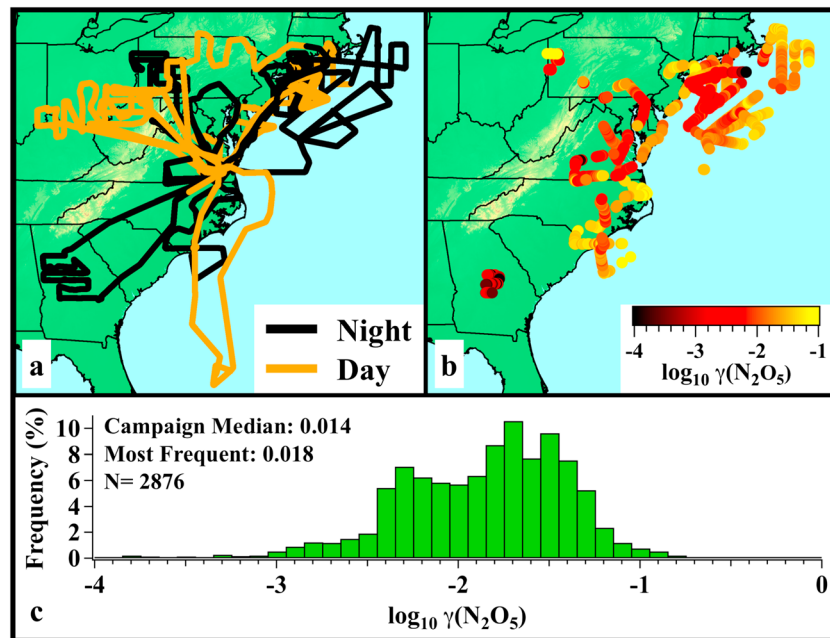


**Figure 3.** (a) Map of WINTER campaign flight tracks over the eastern United States, colored to show day and night (as defined by solar zenith angle  $> 90^\circ$ ) flight periods, which represented 42 and 58% of the data, respectively. The aircraft was based at the NASA Langley campus in coastal Virginia and executed 13 flights of approximately 8 hr duration between 3 February and 13 March 2015. (b) Flight tracks colored by  $\gamma(\text{N}_2\text{O}_5)$ , derived from the box model analysis. (c) Histogram of box model results.

aerosol surface area density (SA) and the mean molecular speed of  $\text{N}_2\text{O}_5$  (c) to calculate  $\gamma(\text{N}_2\text{O}_5)$  and  $\phi(\text{ClNO}_2)$  for every 10-s period. As described later in this section, the 10-s interval was chosen to increase the model computation efficiency while maintaining the spatial resolution ( $\sim 1\text{--}10$  km) of the data products. The remainder of this manuscript will focus on  $\gamma(\text{N}_2\text{O}_5)$  with an analysis of  $\phi(\text{ClNO}_2)$  results planned for an upcoming manuscript.

In this study, SA is assumed constant over each simulation duration and represents the total wet aerosol SA density for particles  $< 3 \mu\text{m}$  in diameter, calculated from measured dry aerosol SA density and RH-dependent SA hygroscopic growth factors for  $< 1 \mu\text{m}$  and  $1\text{--}3 \mu\text{m}$  particles. Base case growth factors were calculated using the Extended-AIM Aerosol Thermodynamics Model (Wexler & Clegg, 2002) for  $1\text{--}3 \mu\text{m}$  aerosol, assuming pure NaCl particles. For  $< 1 \mu\text{m}$  particles, growth factors were calculated using Aerosol Mass Spectrometer (AMS) measurements of dry aerosol mass and estimates of aerosol liquid water (described in section S1 and Figure S1; Attwood et al., 2014; Brock et al., 2016; Cerully et al., 2015; Chang et al., 2010; Jimenez et al., 2009; Mei et al., 2013; Petters & Kreidenweis, 2007; Rickards et al., 2013; Shingler et al., 2016; Suda et al., 2012). Though previous field studies have limited the calculation of  $\gamma(\text{N}_2\text{O}_5)$  to particles  $< 1 \mu\text{m}$  (Bertram, Thornton, Riedel, Middlebrook, et al., 2009; Riedel et al., 2012; Wagner et al., 2013), the small contribution of  $1\text{--}3 \mu\text{m}$  particles (0.5–4%) to total dry SA density will only slightly decrease the WINTER  $\gamma(\text{N}_2\text{O}_5)$  results relative to past studies. Measurements of  $3\text{--}10 \mu\text{m}$  particles were excluded from this analysis due to their small contribution (0–2%) to the total dry SA density. Variations over the simulation duration of SA are not considered here but could lead to an increased variability in derived  $\gamma(\text{N}_2\text{O}_5)$  values. Further discussion of this limitation and additional sensitivities to model assumptions are presented in section 2.2.2.

$$\gamma(\text{N}_2\text{O}_5) = \frac{4 * k_{\text{N}_2\text{O}_5}}{c * \text{SA}} \quad (1)$$

$$\phi(\text{ClNO}_2) = \frac{k_{\text{ClNO}_2}}{k_{\text{N}_2\text{O}_5}} \quad (2)$$

The expression for  $\gamma(\text{N}_2\text{O}_5)$  in (E1) is simplified from that discussed in Fuchs and Sutugin (1970) for conditions where  $\gamma(\text{N}_2\text{O}_5)$  is not limited by gas-phase diffusion to the aerosol surface. According to previous studies (e.g.,

**Table 1**  
Summary of WINTER Observations Used in the Box Model Analysis

Compound	Method/instrument	Accuracy	Meas. frequency	Reference
<i>Gas-Phase Species</i>				
NO	CRDS <sup>a,b</sup>	4%	1 s	Fuchs et al. (2009)
	CL <sup>c</sup>	10%	1 s	Weinheimer et al. (1994)
NO <sub>2</sub>	CRDS <sup>a</sup>	3%	1 s	Fuchs et al. (2009)
	TD-LIF <sup>d</sup>	10%	1 s	Day et al. (2002)
O <sub>3</sub>	CRDS <sup>a</sup>	4%	1 s	Washenfelder et al. (2011)
	CL	5%	1 s	Weinheimer et al. (1994)
NO <sub>y</sub>	CRDS	12%	1 s	Wild et al. (2014)
	CL	50%	1 s	Weinheimer et al. (1994)
N <sub>2</sub> O <sub>5</sub>	CRDS	12%	1 s	Dubé et al. (2006) and Fuchs et al. (2008)
	I-TOF-CIMS <sup>e</sup>	30%	1 s	Lee et al. (2014)
CINO <sub>2</sub>	I-TOF-CIMS	30%	1 s	Lee et al. (2014)
Speciated VOCs	TOGA <sup>f</sup>	< 50%	35 s, 2 min	Apel et al. (2015)
<i>Aerosol Measurements</i>				
Nitrate (<1 μm)	AMS <sup>g</sup>	35%	1 s	DeCarlo et al. (2006)
	PILS-IC <sup>h</sup>	20%	3 min	Guo et al. (2016)
Chloride (<1 μm)	AMS	35%	1 s	DeCarlo et al. (2006)
	PILS-IC	20%	3 min	Guo et al. (2016)
Sulfate (<1 μm)	AMS	35%	1 s	DeCarlo et al. (2006)
Organic (<1 μm)	AMS	35%	1 s	DeCarlo et al. (2006)
Dry surface area Density (<1 μm)	UHSAS <sup>i</sup>	34%	1 s	Cai et al. (2008)
	PCASP <sup>j</sup>	41%	1 s	Strapp et al. (1992)
Dry surface area density (1–3 μm)	PCASP	34%	1 s	Strapp et al. (1992)
<i>Radiative Measurements</i>				
J-values	HARP-AF <sup>k</sup>	<25–40% <sup>k</sup>	10 s	Shetter and Müller (1999)

<sup>a</sup>Excludes research flights 01–04 due to a known problem in the sampling inlet line. <sup>b</sup>NOAA, Cavity Ring Down Spectrometer. <sup>c</sup>NCAR, Chemiluminescence detector. <sup>d</sup>University of California Berkeley, Thermal Dissociation-Laser Induced Fluorescence detector. <sup>e</sup>University of Washington, high-resolution, Time-of-Flight, Iodide Chemical Ionization Mass Spectrometer. <sup>f</sup>NCAR, Trace Organic Gas Analyzer. <sup>g</sup>University of Colorado Boulder, Aerosol Mass Spectrometer. <sup>h</sup>Georgia Institute of Technology, Particle-Into-Liquid Sampler-Ion Chromatography. <sup>i</sup>NCAR, Ultra High Sensitivity Aerosol Spectrometer. <sup>j</sup>NCAR, Passive Cavity Aerosol Spectrometer Probe. <sup>k</sup>HIAPER airborne radiation package-Actinic Flux. For uncertainty description, see supporting information section S1.

Dentener & Crutzen, 1993; Pöschl et al., 2007), this approximation is valid for small particles with diameters less than the N<sub>2</sub>O<sub>5</sub> mean free path (~0.1 μm) or small uptake coefficients (< 0.1). Despite some particle diameters >0.1 μm measured during WINTER (max dN/dlogDp occurred at ≤0.15 μm dry diameter), previous field studies have suggested that correction for diffusion increases derived γ(N<sub>2</sub>O<sub>5</sub>) values by <5% (Aldener et al., 2006).

The box model chemical mechanism included 14 reactions and 15 compounds (see Table 2), chosen as the simplest set of reactions to accurately describe the nocturnal inorganic chemistry of N<sub>2</sub>O<sub>5</sub>. As noted in previous studies, large uncertainties in mechanisms of nocturnal chemistry arise from uncertainties in NO<sub>3</sub> loss reactions (e.g., Phillips et al., 2016; Wagner et al., 2011). In the absence of photochemical radical production, NO<sub>3</sub> serves as one of the primary nocturnal tropospheric oxidants for volatile organic compounds (VOCs). NO<sub>3</sub> also reacts with RO<sub>2</sub> and HO<sub>2</sub> radicals, which can contribute to nocturnal NO<sub>x</sub> recycling (Vaughan et al., 2006). In this analysis, NO<sub>3</sub>-VOC oxidation reactions were lumped and treated as a net NO<sub>x</sub> sink (R12) with a rate constant ( $k_{\text{VOC}}$  [s<sup>-1</sup>]) calculated from WINTER VOCs measured by the Trace Organic Gas Analyzer (TOGA) (described in section S2.1; Atkinson & Arey, 2003; Hjorth et al., 1986). Due to a lack of radical measurements during WINTER, the first-order NO<sub>3</sub> loss rate constant for the NO<sub>x</sub> recycling reaction with HO<sub>2</sub> ( $k_{\text{HO}_2}$  [s<sup>-1</sup>]) (R13) was estimated from the second-order NO<sub>3</sub> + HO<sub>2</sub> reaction rate constant (IUPAC, 2008) and HO<sub>2</sub> concentrations from 2011 over the UK (Stone et al., 2014). These are the most recently reported aircraft observations of HO<sub>2</sub> in the wintertime RL, over a populated region in the Northern Hemisphere. As calculated here,  $k_{\text{HO}_2}$  accounted for 19–50% (36% average) of the model-calculated total NO<sub>3</sub> loss rate constant ( $k_{\text{NO}_3} = k_{\text{HO}_2} + k_{\text{VOC}}$ ), though the overall modeled loss through NO<sub>3</sub> was a relatively small fraction of the total combined loss of N<sub>2</sub>O<sub>5</sub> + NO<sub>3</sub> (11.5% average, see section S3.5). Calculated rate constants for both R12 and



**Table 2**  
Box Model Chemical Mechanism

	Reactants		Products	Rate coefficient expression	Reference/source
R8	NO <sub>2</sub> + O <sub>3</sub>	→	NO <sub>3</sub> + O <sub>2</sub>	$k_8 = 1.4 \times 10^{-13} e^{(-2470/\text{Temp})} [\text{cm}^3 \text{ molecule}^{-1} \text{ s}^{-1}]$	IUPAC 2012
R9f	NO <sub>3</sub> + NO <sub>2</sub>	→	N <sub>2</sub> O <sub>5</sub>	$k_{9f} = (k_0/k_\infty) * F / (k_0 + k_\infty) [\text{cm}^3 \text{ molecule}^{-1} \text{ s}^{-1}]^a$	IUPAC 2012
R9r	N <sub>2</sub> O <sub>5</sub>	→	NO <sub>3</sub> + NO <sub>2</sub>	$k_{9r} = (k_0/k_\infty) * F / (k_0 + k_\infty) [\text{cm}^3 \text{ molecule}^{-1} \text{ s}^{-1}]^b$	IUPAC 2012
R10	N <sub>2</sub> O <sub>5</sub> + aerosol	→	2 HNO <sub>3</sub>	$k_{10} = k_{\text{HNO}_3} [\text{s}^{-1}]$	Model derived
R11	N <sub>2</sub> O <sub>5</sub> + aerosol	→	HNO <sub>3</sub> + ClNO <sub>2</sub>	$k_{11} = k_{\text{ClNO}_2} [\text{s}^{-1}]$	Model derived
R12	NO <sub>3</sub> + VOC	→	Products	$k_{12} = k_{\text{VOC}} [\text{s}^{-1}]$	Measured <sup>c</sup>
R13	NO <sub>3</sub> + HO <sub>2</sub>	→	NO <sub>2</sub> + OH + O <sub>2</sub>	$k_{13} = k_{\text{HO}_2} = 1.2 \times 10^{-4} [\text{s}^{-1}]$	(Stone et al., 2014) <sup>d</sup>
R14	NO <sub>3</sub> + NO	→	2 NO <sub>2</sub>	$k_{14} = 1.80 \times 10^{-11} e^{(110/\text{Temp})} [\text{cm}^3 \text{ molecule}^{-1} \text{ s}^{-1}]$	IUPAC, 2008
R15	NO + O <sub>3</sub>	→	NO <sub>2</sub> + O <sub>2</sub>	$k_{15} = 2.07 \times 10^{-12} e^{(-1400/\text{Temp})} [\text{cm}^3 \text{ molecule}^{-1} \text{ s}^{-1}]$	IUPAC 2013
R16	O <sub>3</sub> + <i>hν</i>	→	O + O <sub>2</sub>	$k_{16} = j(\text{O}^1\text{D})$	Measured
R17	NO <sub>2</sub> + <i>hν</i>	→	NO + O	$k_{17} = j(\text{NO}_2)$	Measured
R18	NO <sub>3</sub> + <i>hν</i>	→	NO <sub>2</sub> + O	$k_{18} = j(\text{NO}_3)$	Calculated <sup>e</sup>
R19	N <sub>2</sub> O <sub>5</sub> + <i>hν</i>	→	NO <sub>2</sub> + NO <sub>3</sub>	$k_{19} = j(\text{N}_2\text{O}_5)$	Measured
R20	ClNO <sub>2</sub> + <i>hν</i>	→	Cl + NO <sub>2</sub>	$k_{20} = j(\text{ClNO}_2)$	Measured

<sup>a</sup> $k_0 = 3.6 \times 10^{-30} M^*(\text{Temp}/300)^{-4.1}$ ,  $k_\infty = 1.9 \times 10^{-12} M^*(\text{Temp}/300)^{0.2}$ ,  $\text{KR} = k_0/k_\infty$ ,  $\text{NC} = 0.75 - 1.27 \log_{10}(0.35)$ ,  $F = 10^{(\log_{10}(0.35)/(1 + \log_{10}(\text{KR}/\text{NC})^2))}$ ,  $M$  = Pressure [mbar]  $1 \times 10^{-4} / (k_b * \text{Temp})$ . <sup>b</sup> $k_0 = 1.3 \times 10^{-33} M^*(\text{Temp}/300)^{-3.5} e^{(-11,000/\text{Temp})}$ ,  $k_\infty = 9.7 \times 10^{-14} M^*(\text{Temp}/300)^{0.1} e^{(-11080/\text{Temp})}$ ,  $\text{KR} = k_0/k_\infty$ ,  $\text{NC} = 0.75 - 1.27 \log_{10}(0.35)$ ,  $F = 10^{(\log_{10}(0.35)/(1 + \log_{10}(\text{KR}/\text{NC})^2))}$ . <sup>c</sup>Described in section S2.1. <sup>d</sup>Described in section 2.2.1. <sup>e</sup>Described in section S2.3.

R13 were treated as constants throughout each simulation duration, which has the potential to add variability to the  $\gamma(\text{N}_2\text{O}_5)$  results since VOC reactivity is likely to decrease with time via depletion of reactive VOCs. NO<sub>3</sub> reactions with RO<sub>2</sub> were not explicitly included in this mechanism due to a lack of wintertime RO<sub>2</sub> aircraft field measurements. If this treatment were to result in  $k_{\text{NO}_3}$  values outside the bounds of uncertainty already considered (described below), derived  $\gamma(\text{N}_2\text{O}_5)$  values would be reduced. Direct NO<sub>3</sub> uptake was also excluded from the mechanism since reported NO<sub>3</sub> uptake coefficients are generally small on inorganic aerosol ( $\gamma(\text{NO}_3) \sim 10^{-3}$ ; Brown & Stutz, 2012), which dominated the WINTER aerosol composition (Figure 6). Some analyses, however, have suggested larger values of NO<sub>3</sub> uptake onto organic surfaces (Mao et al., 2013; Ng et al., 2017). NO<sub>3</sub> uptake coefficients of  $\leq 0.1$  would decrease the median  $\gamma(\text{N}_2\text{O}_5)$  by  $< 10\%$  (section S3.5). Due to the multiple sources of uncertainty in  $k_{\text{NO}_3}$  (including VOC measurements, HO<sub>2</sub>/RO<sub>2</sub> reactions, and NO<sub>3</sub> uptake), reactivity values calculated here are likely lower limits. The box model, however, displayed the smallest sensitivity of all parameters tested to  $k_{\text{NO}_3}$  (Table S5), with the campaign-median changing by  $-1.0/+1.2\%$  in response to  $\pm 10\%$  changes in both  $k_{\text{VOC}}$  and  $k_{\text{HO}_2}$ . To more accurately represent the total  $k_{\text{NO}_3}$  uncertainty, model sensitivities to  $\pm 50\%$  changes in  $k_{\text{NO}_3}$  ( $-5.0/+6.0\%$  change in median) were included in the total error calculation of each individual  $\gamma(\text{N}_2\text{O}_5)$  value (described in section 3.1). Relative to previous field studies (e.g., Phillips et al., 2016), this small  $\gamma(\text{N}_2\text{O}_5)$  sensitivity to direct NO<sub>3</sub> loss is explained in part by low NO<sub>3</sub> mixing ratios, as a result of cold winter temperatures that favor N<sub>2</sub>O<sub>5</sub> in its equilibrium with NO<sub>3</sub>, and in part because of low biogenic emissions, which are typically the largest class of VOCs that contribute to NO<sub>3</sub> reactivity in continental regions (e.g., Aldener et al., 2006; Brown & Stutz, 2012). For one WINTER flight, however, relatively warmer temperatures did increase the sensitivity of modeled  $\gamma(\text{N}_2\text{O}_5)$  to  $k_{\text{NO}_3}$  ( $-25.2\%/+3.5\%$  to  $\pm 10\%$  changes, discussed in section S3.5). As  $k_{\text{NO}_3}$  values here are likely lower limits, an increase in NO<sub>3</sub> reactivity on this flight would serve to decrease  $\gamma(\text{N}_2\text{O}_5)$  below the original values of  $< 1 \times 10^{-3}$ . This flight highlights the fact that this particular model is most appropriate (has the lowest uncertainties) under cold, wintertime conditions with low NO<sub>3</sub> reactivity. As a result of the small  $k_{\text{NO}_3}$  sensitivity on all other flights, more explicit treatment of NO<sub>3</sub> chemistry was not required for this mechanism to accurately simulate nocturnal N<sub>2</sub>O<sub>5</sub> chemistry during WINTER.

Additional N<sub>2</sub>O<sub>5</sub> loss through direct homogeneous (i.e., gas phase) hydrolysis with water vapor (Mentel et al., 1996; Wahner, Mentel, & Sohn, 1998) was not included in the mechanism. Parameterized WINTER homogeneous reaction rate constants ( $k_{\text{Homo}} = k_{\text{Total N}_2\text{O}_5} - k_{\text{Uptake}}$ , SE5) were predicted to be  $\sim 10$  times lower than total  $k_{\text{N}_2\text{O}_5}$  values, derived from the box model (Figure S3). Additional inconsistencies between calculated  $k_{\text{Homo}}$  and observed  $k_{\text{N}_2\text{O}_5}$  values in previous summertime studies suggest that the current parameterization may actually overpredict  $k_{\text{Homo}}$ , despite the low values here (Aldener et al., 2006; Brown et al., 2006; Brown

et al., 2009). This result is not only consistent with parameterized values that exceed the smallest WINTER loss rate constants (Figure S3), but also suggests that homogeneous loss is a minor contributor to total  $\text{N}_2\text{O}_5$  loss.

Each simulation was initialized at the onset of nocturnal  $\text{N}_2\text{O}_5$  production and forward integrated, assuming constant reaction rate coefficients and SA (section 2.2.2), until the time of aircraft measurement. As defined by Wagner et al. (2013), the simulation start time was set as the time of sunset ( $\text{SZA} = 90^\circ$ ), while duration was the time elapsed between sunset and measurement. These definitions make two additional assumptions: (1) nocturnally dominant  $\text{N}_2\text{O}_5$  chemistry began exactly at sunset and (2) air measured from the aircraft in the RL has been decoupled from the surface since sunset (i.e., not influenced by surface  $\text{NO}_x$  emissions). In reality, low actinic flux and cold temperatures allow concentrations of nocturnal species such as  $\text{N}_2\text{O}_5$  to start building up before sunset (i.e.,  $\text{SZA} < 90^\circ$ ). In addition, a delayed decoupling of the residual and surface layers would allow  $\text{NO}_x$  emissions to mix into the RL after sunset. Both assumptions were accounted for in this analysis by calculating a simulation start time (i.e., onset of  $\text{N}_2\text{O}_5$  buildup) and duration (i.e., air age) using a combination of the calculated  $\text{N}_2\text{O}_5$  daytime steady state lifetime and the observed  $\text{NO}_2/\text{NO}_y$  ratio, described in extensive detail in section S2.3. Despite uncertainties associated with these calculations, sensitivities of the box model to changes in both start time and duration were small relative to base case assumptions ( $\Delta\text{median } \gamma(\text{N}_2\text{O}_5) < 7.1\%$ ).

Once the simulation start time and duration were determined, the model used three main steps (illustrated in Figure S2) to derive  $k_{\text{ClNO}_2}$  and  $k_{\text{N}_2\text{O}_5}$  by iteratively fitting final simulated mixing ratios to aircraft observations of  $\text{NO}_2$ ,  $\text{O}_3$ ,  $\text{N}_2\text{O}_5$ , and  $\text{ClNO}_2$ . The first step holds  $k_{\text{N}_2\text{O}_5}$  constant at an initial value of  $1 \times 10^{-4} \text{ s}^{-1}$ ,  $k_{\text{ClNO}_2}$  at  $0 \text{ s}^{-1}$ , and iteratively adjusts the initial concentrations of  $\text{NO}_2$  (or  $\text{NO}$ ) and  $\text{O}_3$  until the final simulated mixing ratios are within 0.5% of the observed values. The second step holds these derived-initial concentrations constant while iteratively adjusting  $k_{\text{N}_2\text{O}_5}$  until the simulated  $\text{N}_2\text{O}_5$  is within 1% of the aircraft-observed mixing ratio. Steps 1 and 2 are repeated until  $\text{NO}_2$ ,  $\text{O}_3$ , and  $\text{N}_2\text{O}_5$  simultaneously meet their respective fit criteria (i.e., 0.5% for  $\text{O}_3$  and  $\text{NO}_2$  and 1% for  $\text{N}_2\text{O}_5$ ). The third step holds all derived parameters constant while iteratively adjusting  $k_{\text{ClNO}_2}$  until the final simulated mixing ratio of  $\text{ClNO}_2$  is within 1% of observations. This process was repeated with a 10-s resolution during all WINTER flights with  $\text{SZA} > 90^\circ$ . Although chemical measurements were collected at a 1-Hz resolution, data were averaged to 10 s to improve the model's computational efficiency and reduce scatter in the  $\gamma(\text{N}_2\text{O}_5)$  and  $\phi(\text{ClNO}_2)$  products, while maintaining their spatial resolution of  $\sim 1$ –10 km. The instrument-specific observations used as fit parameters varied by flight and are listed in Table S4. Correlation plots of all overlapping measurements in section S3.2 indicate agreement to within 12% for all species. An additional 45 model simulations suggest a small sensitivity ( $< 20\%$ ) in  $\gamma(\text{N}_2\text{O}_5)$  to measurement accuracies and instrument choice, except for the two  $\text{N}_2\text{O}_5$  measurements, as discussed in section S3.2.3.

### 2.2.2. Model Filters, Limitations, and Additional Sensitivity Studies

As previously mentioned, simulations were limited to aircraft measurements within the RL ( $\text{SZA} > 90^\circ$ ), at altitudes below the free troposphere (typically  $\sim 1,000$  m above ground level) and above the nocturnal boundary layer (estimated to be  $\sim 100$  m above ground level) (Stull, 1988) in order to focus on nocturnal air that had been in contact with surface emissions the previous day. The depth of the RL was time and location dependent and determined throughout each flight using the altitude of inversions (i.e., steeper increases in potential temperature with height) observed during vertical profiles. Data were additionally filtered to remove points with reported RH  $> 95\%$  (1.7% of derived values) due to uncertainty in the aerosol hygroscopic growth curve at high RH (section S1).

One limitation of this box model is that nonconvergence occurs as  $k_{\text{N}_2\text{O}_5}$  approaches zero (minimum  $2 \times 10^{-7} \text{ s}^{-1}$ ), due to an increased sensitivity to uncertainties in chemical fit parameters. Absence of data close to this limit biases the WINTER median  $\gamma(\text{N}_2\text{O}_5)$  high. Of the total number of derived  $k_{\text{N}_2\text{O}_5}$  values for WINTER, 245 or 8% did not converge. Model nonconvergence occurred on five of the nine flights, with the majority occurring on RF10. The maximum bias introduced from this nonconvergence is relatively small and does not change the main conclusions presented in later sections. For example, assuming a value of 0 for all nonconverging points decreases the campaign median  $\gamma(\text{N}_2\text{O}_5)$  by  $< 12\%$ . Due to the small bias compared to the total 4 orders-of-magnitude range in model-predicted values, these points are not further considered. A second limitation is that the model cannot account for time-varying changes in SA or reaction rate constants, as mentioned previously in section 2.2.1. For example, assuming a constant value for  $\text{NO}_3$ -VOC reactivity, which may decrease overtime, could lead to an overprediction in  $\gamma(\text{N}_2\text{O}_5)$  at longer simulation

durations and underprediction at shorter times. In addition,  $\gamma(\text{N}_2\text{O}_5)$  itself and aerosol SA could change with time, although simulation duration did not show a statistically significant ( $p > 0.05$ ) correlation with aerosol size and showed a weak correlation ( $r^2 = 0.20$ ) with other contributing factors such as aerosol nitrate (section 4.2). The possible increase in SA over time was estimated for each point by assuming that all nitrate formed in the model from  $\text{N}_2\text{O}_5$  uptake resulted in aerosol-phase nitrate. This method provides an upper limit to the potential change in SA from  $\text{N}_2\text{O}_5$  uptake as aerosol thermodynamics are expected to partition some fraction of this nitrate to gas-phase nitric acid. The average SA increase from nitrate accumulation was 5.0% for all WINTER flights with a maximum of 24.5%. These upper limit percent changes are well within the uncertainty of the SA measurement (Table 1) included in the total error analysis (section 3.1) and are therefore not considered further. At least one of these factors, however, likely contributes to the negative correlation observed between WINTER  $\gamma(\text{N}_2\text{O}_5)$  values and simulation duration (Figure S20) but cannot be confirmed with available aircraft data and may serve to increase the variability in the literature parameterization comparisons presented in section 4.3.2.

To test the robustness of the box model to uncertainties in model parameters and assumptions described above, a series of 18 sensitivity studies were additionally conducted for each WINTER flight. A summary of resulting changes in campaign-median  $\gamma(\text{N}_2\text{O}_5)$  values is provided in Table S5. Resulting median  $\gamma(\text{N}_2\text{O}_5)$  values showed small ( $< 11\%$ ) sensitivities to uncertainties in air age (duration), simulation start time, aerosol hygroscopic growth factor,  $\text{NO}_3$  reactivity, photolysis frequencies, and  $\text{O}_3$  measurements but larger sensitivities ( $> 20\%$ ) to uncertainties in measured dry aerosol SA density,  $\text{NO}_2$ , and  $\text{N}_2\text{O}_5$ . Data collected over the ocean (defined by the GPS coordinates of the eastern United States shoreline) were additionally tested for sensitivities to  $\text{N}_2\text{O}_5$  ocean surface deposition (rate calculated from Kim et al., 2014) and dilution and showed  $-14\%$  and  $-5.7\%$  changes, respectively. Additional information (e.g., Seidel et al., 2012; Sickles & Shadwick, 2007) and results for all sensitivity studies are in section S3 in the supporting information.

### 3. Results

#### 3.1. Box Model Results— $\gamma(\text{N}_2\text{O}_5)$

Figure 3b shows WINTER flight tracks colored by model-derived  $\gamma(\text{N}_2\text{O}_5)$ , with a histogram illustrating the campaign-wide distribution in Figure 3c. As described, the box model derived 2,876, 10-s averaged, individual  $\gamma(\text{N}_2\text{O}_5)$  determinations over the course of 9 WINTER flights, providing the first regional-scale determinations of  $\gamma(\text{N}_2\text{O}_5)$  during a single winter season, as well as over 50 times more individual  $\gamma(\text{N}_2\text{O}_5)$  determinations than all previous aircraft studies combined (see Figure 4) (Brown et al., 2006; Brown et al., 2009; Morgan et al., 2015). In addition, the model accounted for 35% of all nocturnal RL data collected during WINTER, compared to 7% from 25 days of continuous sampling in 2011 at a Colorado ground site (Wagner et al., 2013).

Over this single, 5-week period,  $\gamma(\text{N}_2\text{O}_5)$  ranged 4 orders of magnitude from  $2 \times 10^{-5}$  to 0.1751 with median value of 0.0143 ( $1\sigma \pm 0.007$  or  $\pm 52\%$ ), which is within 43% of where GEOS-Chem model estimates of  $\text{O}_3$  and OH are most sensitive to  $\gamma(\text{N}_2\text{O}_5)$  (Macintyre & Evans, 2010) (Figure 4). The histogram in Figure 3c shows the most frequent value occurred at 0.018 and a secondary peak at a lower value of 0.004. Figure 3b does not show a strong geographical dependence in  $\gamma(\text{N}_2\text{O}_5)$ , with continental and marine flights encompassing the same range (Figure S21). Marine flights, however, could have been largely influenced by continental emission sources due to persistent offshore winds during WINTER.

Errors for each individual point are shown by flight in Figure S22, calculated from the quadrature addition of measurement uncertainties ( $\text{NO}_2$ ,  $\text{O}_3$ ,  $\text{N}_2\text{O}_5$ , and dry SA density, Table 1) and model sensitivities to the aerosol hygroscopic growth factor, 50% changes in  $k_{\text{NO}_3}$  (50% in  $k_{\text{VOC}}$  and  $k_{\text{HO}_2}$ ), air age, and start time (Table S5). In addition to Figure S22, time series from three different flights (continental and marine) in Figure S23 illustrate the observed variability in  $\gamma(\text{N}_2\text{O}_5)$  and associated variables within and between different parcels of air.

The majority of smallest  $\gamma(\text{N}_2\text{O}_5)$  values ( $< 10^{-3}$ , discussed further in sections 2.2.1, 4.3.2, S3.5, and S7) were derived on research flight 10. These are lower than many values previously reported by field and laboratory studies and are most sensitive to changes in  $k_{\text{NO}_3}$ . Despite a small sensitivity of the campaign median to  $k_{\text{NO}_3}$  ( $\sim 5\%$  change in  $\gamma(\text{N}_2\text{O}_5)$  for a 50% change in  $k_{\text{NO}_3}$ ), these particular points are reduced from values  $\sim 1 \times 10^{-3}$  to as low as  $2 \times 10^{-5}$  if total  $\text{NO}_3$  reactivity ( $k_{\text{VOC}} + k_{\text{HO}_2}$ ) is increased by 50% (to account for possible sources of



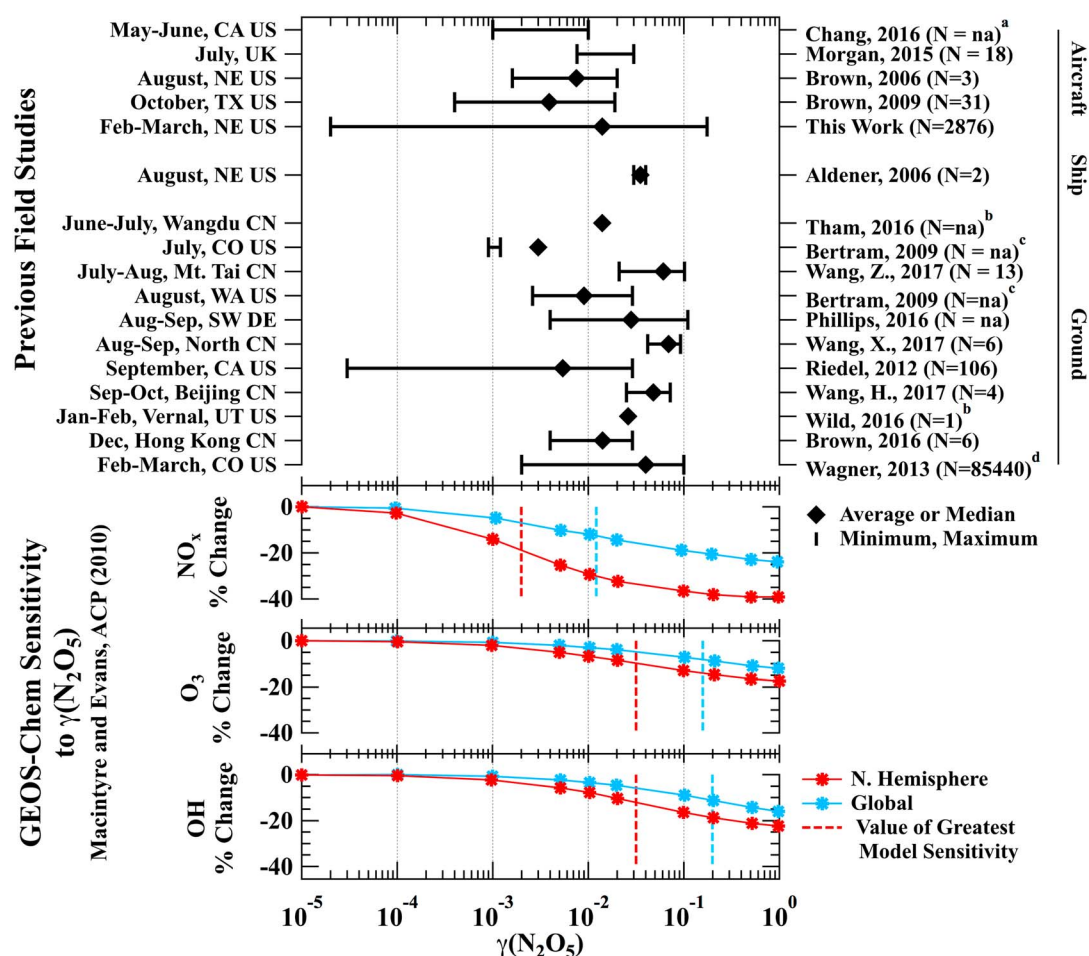


**Figure 4.** Previous field determinations of  $\gamma(\text{N}_2\text{O}_5)$  in comparison to OH, O<sub>3</sub>, and NO<sub>x</sub> sensitivities in GEOS-Chem, data courtesy of Mat Evans (Macintyre & Evans, 2010). *N* represents the number of points in each study, if reported. <sup>a</sup>Approximate range, exact values not reported. <sup>b</sup>Range not reported. <sup>c</sup>Average not reported, diamond represents the median; minimum and maximum values not reported, 25th and 75th percentiles shown instead. <sup>d</sup>Average and median not reported, diamond represents the most frequent value.

missing  $k_{\text{NO}_3}$ , section S3.5). All additional sources of error, including measurement uncertainties, were small for these values as they were derived when fitting the model to the largest concentrations of  $\text{N}_2\text{O}_5$  (Figure 6). Despite the increased sensitivity to  $k_{\text{NO}_3}$ , it remains important to derive and distinguish  $\gamma(\text{N}_2\text{O}_5)$  values in this range as GEOS-Chem results (lower panel in Figure 4) show that oxidants and NO<sub>x</sub> remain sensitive to  $\gamma(\text{N}_2\text{O}_5)$  down to values of  $1 \times 10^{-5}$ . It is additionally important to identify the physical cause of these lowest values as  $\gamma(\text{N}_2\text{O}_5)$  values in this range are not typically predicted by  $\gamma(\text{N}_2\text{O}_5)$  parameterizations based on the current mechanistic understanding of  $\text{N}_2\text{O}_5$  uptake (section 4).

An additional comparison of box model results to  $\gamma(\text{N}_2\text{O}_5)$  values calculated from WINTER GEOS-Chem simulations (described in section S4 and Figure S24; Fountoukis & Nenes, 2007; Hodzic & Jimenez, 2011; Kim et al., 2015; Pye et al., 2009) shows (1) no spatial, systematic trend in the percent differences between the two determinations, (2) a smaller range in GEOS-Chem-derived  $\gamma(\text{N}_2\text{O}_5)$  values relative to the box model, and (3) a 25.3% lower median value in GEOS-Chem. While a discussion of differences between GEOS-Chem and box model results (sources include deposition, dilution, aerosol composition, and surface area) is outside the scope of this manuscript, a  $\gamma(\text{N}_2\text{O}_5)$  parameterization similar to that used in GEOS-Chem (section S4) is discussed with other literature parameterizations in section 4.3.2.

WINTER  $\gamma(\text{N}_2\text{O}_5)$  values are shown in comparison to all previous field determinations of  $\gamma(\text{N}_2\text{O}_5)$  in the upper panel of Figure 4 (and Table S6). The 4 order-of-magnitude range in WINTER values encompasses all values

previously reported, despite a large variability in previous sample locations, platforms, and seasons. Using the nocturnal steady state approximation, previous aircraft studies have reported  $\gamma(\text{N}_2\text{O}_5)$  values ranging from 0.001 to 0.02 over the northeast United States in August 2004 (Brown et al., 2006),  $4 \times 10^{-4}$  to 0.019 over Texas in October 2006 (Brown et al., 2009), 0.001 to 0.01 over California in May and June 2010 (Chang et al., 2016), and 0.0076 to 0.03 over northwestern Europe/UK in July 2010 (Morgan et al., 2015). These values largely fall within the lower population of WINTER  $\gamma(\text{N}_2\text{O}_5)$  values (Figure 3c). Multiple studies have also derived  $\gamma(\text{N}_2\text{O}_5)$  values ranging from  $3 \times 10^{-5}$  to 0.11 (see Table S6) using flow reactors and the steady state approximation during both summer and fall seasons from a ship (Aldener et al., 2006) and multiple ground sites in the United States (Bertram, Thornton, Riedel, Middlebrook, et al., 2009; Riedel et al., 2012), Europe (Phillips et al., 2016), and China (Tham et al., 2016; H. Wang et al., 2017; Z. Wang et al., 2017; X. Wang et al., 2017). Few studies, and none from aircraft, have reported  $\gamma(\text{N}_2\text{O}_5)$  values during the winter season, where colder temperatures and low  $\text{NO}_3$  reactivities are expected to increase nocturnal  $\text{N}_2\text{O}_5$  production and lifetime relative to warmer seasons. Using a box model approach, Wagner et al. (2013) derived  $\gamma(\text{N}_2\text{O}_5)$  values between 0.002 and 0.1 in Weld County, Colorado in February–March 2011, Wild et al. (2016) fit an average  $k_{\text{N}_2\text{O}_5}$  (in E1) value to that predicted by the steady state approximation to derive single value of 0.026 for January–February 2012 in rural Utah, and Brown et al. (2016) used the steady state approximations to derive values between 0.004 and 0.029 in Hong Kong, China during December 2013. An additional analysis of the  $\text{N}_2\text{O}_5$  lifetime ( $(k_{\text{N}_2\text{O}_5})^{-1}$ ) near Fairbanks, Alaska showed that  $\text{N}_2\text{O}_5$  loss may be enhanced by the presence of ice surfaces at high latitudes during winter (Apodaca et al., 2008). Comparison between all past field studies in Figure 4 does not indicate a strong seasonal dependence of  $\gamma(\text{N}_2\text{O}_5)$  nor bias from sampling platform type (i.e., aircraft, ship, or ground) or analysis method.

To provide a broader context for all field determinations of  $\gamma(\text{N}_2\text{O}_5)$ , the lower panel of Figure 4 shows the GEOS-Chem-predicted sensitivity (from Macintyre and Evans, 2010) of tropospheric oxidants ( $\text{O}_3$ , OH) and  $\text{NO}_x$  to changes in  $\gamma(\text{N}_2\text{O}_5)$ , both globally (blue) and in the Northern Hemisphere (red). These results show that  $\text{N}_2\text{O}_5$  uptake can lead to >15% reductions in OH and  $\text{O}_3$  and 40% reductions in  $\text{NO}_x$  over the  $\gamma(\text{N}_2\text{O}_5)$  range of  $1 \times 10^{-5}$  to 1, with vertical lines corresponding to the values of greatest model sensitivity (greatest  $\Delta\text{oxidant}/\Delta\gamma(\text{N}_2\text{O}_5)$ ). Nearly all previous field determinations, and 95% of WINTER values, fall between 0.002 and 0.2, encompassing the range where global and regional annual burdens of  $\text{NO}_x$ , OH, and  $\text{O}_3$  display a maximum sensitivity to  $\gamma(\text{N}_2\text{O}_5)$  (Macintyre & Evans, 2010), highlighting the importance of developing and incorporating an accurate and robust  $\gamma(\text{N}_2\text{O}_5)$  parameterization into 3-D chemical transport models.

### 3.2. Comparison to the Steady State Approximation

The nocturnal steady state approximation has been the most common method for deriving  $\gamma(\text{N}_2\text{O}_5)$  from ambient observations of  $\text{O}_3$ ,  $\text{NO}_2$ , and  $\text{N}_2\text{O}_5$  (Table S6). Despite its successful application to previous field data (Aldener et al., 2006; Brown et al., 2006, 2009, 2016; Chang et al., 2016; Morgan et al., 2015; Phillips et al., 2016; Tham et al., 2016; H. Wang et al., 2017; Z. Wang et al., 2017; X. Wang et al., 2017) and relative simplicity relative to the iterative box model, this approach can fail under cold temperatures, high  $\text{NO}_2$  concentrations, and small sinks for both  $\text{N}_2\text{O}_5$  and  $\text{NO}_3$  (Brown et al., 2003). To evaluate the applicability of this method to WINTER data, this section compares model-derived  $\gamma(\text{N}_2\text{O}_5)$  values to those estimated assuming steady state concentrations of  $\text{N}_2\text{O}_5$ .

The nocturnal steady state lifetime of  $\text{N}_2\text{O}_5$  ( $\tau_{\text{ss}}(\text{N}_2\text{O}_5)$ ) is shown in (E3). The equilibrium rate constant for Reactions (R9f) and (R9r) (Table 2) is given by  $K_{\text{eq}}$ ;  $k_{\text{VOC}}$  is the first-order loss rate constant of  $\text{NO}_3$  (R12), and  $k_{\text{N}_2\text{O}_5}$  is the total loss rate constant of  $\text{N}_2\text{O}_5$  (R10 + R11). Substituting the expression relating  $k_{\text{N}_2\text{O}_5}$  and  $\gamma(\text{N}_2\text{O}_5)$  from (E1), (E3) can be rearranged to (E4) to solve for the steady state approximation of  $\text{N}_2\text{O}_5$  uptake ( $\gamma_{\text{ss}}(\text{N}_2\text{O}_5)$ ) using ambient measurements of total wet aerosol SA density,  $\text{N}_2\text{O}_5$ ,  $\text{NO}_2$ , and  $\text{O}_3$ .

$$\tau_{\text{ss}}(\text{N}_2\text{O}_5)^{-1} = \frac{k_8[\text{NO}_2][\text{O}_3]}{[\text{N}_2\text{O}_5]} \approx (k_{\text{N}_2\text{O}_5}) + \frac{k_{\text{VOC}}}{K_{\text{eq}}[\text{NO}_2]} \quad (3)$$

$$\gamma_{\text{ss}}(\text{N}_2\text{O}_5)0.25\text{cSA} = \frac{k_8[\text{NO}_2][\text{O}_3]}{[\text{N}_2\text{O}_5]} - \frac{k_{\text{VOC}}}{K_{\text{eq}}[\text{NO}_2]} \quad (4)$$

Results in Figure 5a show that the steady state approximation generally overpredicts  $\gamma(\text{N}_2\text{O}_5)$  with a slope of 1.13, relative to the box model, which does not make assumptions about steady state. Figure 5c shows the

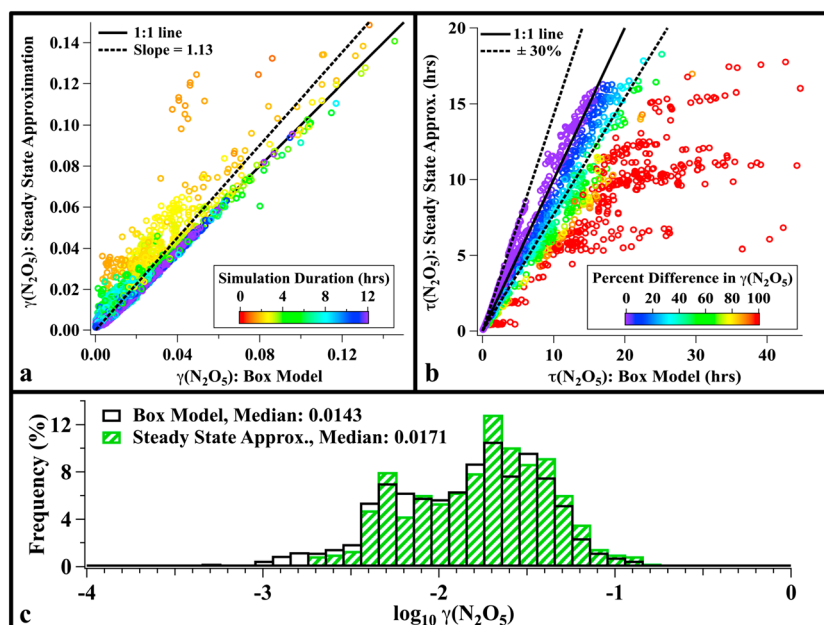


**Figure 5.** Comparison of iterative box model and steady state approximation. (a) Comparison of WINTER  $\gamma(\text{N}_2\text{O}_5)$  values, colored by simulation duration. (b) Comparison of WINTER  $\text{N}_2\text{O}_5$  lifetimes, colored by percent difference between box model and steady state predicted  $\gamma(\text{N}_2\text{O}_5)$  values. (c) Histogram comparing box model results to those derived by the steady state approximation.

distributions of the two derivation methods, with a 20% larger median predicted by the steady state approximation than the original box model. The color scale in Figure 5a shows that agreement between the model and the steady state approximation is generally better for older air (i.e., longer simulation duration). Disagreement at the lowest  $\gamma(\text{N}_2\text{O}_5)$  values may be driven by high measured  $\text{NO}_x$  that keeps the system from reaching equilibrium despite long simulation times (not shown).

Figure 5b shows the steady state  $\text{N}_2\text{O}_5$  lifetime ( $(k_{\text{N}_2\text{O}_5})^{-1}$ ) calculated from (E3) against the box model-predicted lifetime. Under steady state, these lifetimes should be equivalent to within 30% due to combined instrument sampling uncertainties for  $\text{N}_2\text{O}_5$ ,  $\text{O}_3$ , and  $\text{NO}_2$  (Table 1). Despite the wintertime, high- $\text{NO}_x$  conditions, Figure 5b indicates that the steady state approximation was valid (i.e.,  $(k_{\text{N}_2\text{O}_5})^{-1}$  within 30% of the box model) for 65% of the model-derived points. During these times, the percent difference between the box model and steady state calculated  $\gamma(\text{N}_2\text{O}_5)$  values was largely less than 40% (Figure 5b, color scale). The box model analysis, however, is applicable to a wider range of conditions and includes additional  $\text{NO}_2$  recycling reactions (R13) and is therefore a more accurate representation of the WINTER data.

## 4. Discussion

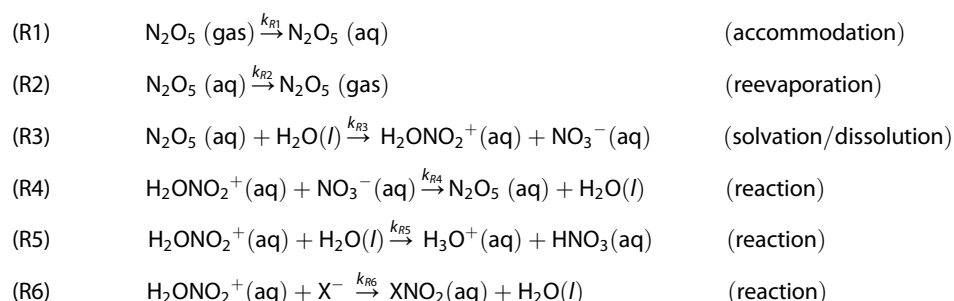
### 4.1. Model Mechanism Background

The expression for  $\gamma(\text{N}_2\text{O}_5)$  in (E1) does not provide any information about the mechanistic factors controlling uptake, required for the development of a predictive parameterization for regional/global 3-D models. As briefly described here, and in further detail elsewhere (Davidovits et al., 2006; Kolb et al., 2002; Pöschl et al., 2007, and references therein),  $\gamma(\text{N}_2\text{O}_5)$  has been described using a resistor model framework with decoupled, individual processes represented in terms of their resistance to uptake ( $1/\Gamma$ ). Using this approach, the net uptake coefficient is represented in equation (E5) by adding, in series, the conductance terms ( $\Gamma$ ) for the processes of (1) gas-phase diffusion ( $\Gamma_{\text{diff}}$ ), (2) surface mass accommodation ( $\alpha$ ), and the parallel processes of (3) bulk-phase solubility ( $\Gamma_{\text{sol}}$ ) and (4) reaction ( $\Gamma_{\text{rxn}}$ ). In accordance with this model framework, net  $\gamma(\text{N}_2\text{O}_5)$  increases with decreasing resistance but is ultimately controlled by the individual process that has the largest resistance (smallest  $\Gamma$ ) to uptake.

$$\frac{1}{\gamma(\text{N}_2\text{O}_5)} = \frac{1}{\Gamma_{\text{diff}}} + \frac{1}{\alpha} + \frac{1}{\Gamma_{\text{sol}} + \Gamma_{\text{rxn}}} \quad (5)$$

Previous studies have proposed that both  $\alpha$  and  $\Gamma_{\text{sol}}$  or  $\Gamma_{\text{rxn}}$  can act as the limiting process under certain conditions, which may change as a function of aerosol composition and availability of liquid water (e.g., Badger et al., 2006; Bertram & Thornton, 2009; Folkers et al., 2003; Griffiths & Cox, 2009; Hallquist et al., 2000; Thornton & Abbatt, 2005). The probability of surface accommodation may be impacted by surface-specific conditions such as surfactant organic coatings (e.g., Thornton & Abbatt, 2005) and temperature (e.g., Griffiths & Cox, 2009; Hallquist et al., 2000). Specific factors controlling  $\Gamma_{\text{sol}}$  and/or  $\Gamma_{\text{rxn}}$  can be further analyzed through the chemical mechanism provided by mechanistic reactions (R1)–(R6), discussed in detail by Bertram and Thornton (2009) and reviewed by Chang et al. (2011). The chemical mechanism, shown diagrammatically in relation to the resistor model in Figure 2, indicates that  $\Gamma_{\text{sol}}$  and  $\Gamma_{\text{rxn}}$  ((R3)–(R6)) are dependent on factors such as aerosol water and the availability of bulk-phase nucleophiles.

In order to evaluate the agreement between the laboratory-based mechanism and field-derived results, the following sections analyze the trends in WINTER  $\gamma(\text{N}_2\text{O}_5)$  values with each individual factor thought to contribute to uptake resistance. WINTER  $\gamma(\text{N}_2\text{O}_5)$  results are then compared to previously derived parameterizations for  $\gamma(\text{N}_2\text{O}_5)$  to inform an empirical, field-derived parameterization for  $\gamma(\text{N}_2\text{O}_5)$  on ambient aerosol, further used to evaluate the current mechanistic understanding of  $\text{N}_2\text{O}_5$  uptake.



## 4.2. Dependence of $\gamma(\text{N}_2\text{O}_5)$ on Controlling Variables

The large number of data points and wide spatial domain during WINTER provide the most comprehensive test to date of the ability of lab-based  $\gamma(\text{N}_2\text{O}_5)$  parameterizations to reproduce field observations. This comparison has been previously limited to a small number of data points and/or single locations that reduce variability in relevant factors (e.g., aerosol nitrate) (Brown et al., 2009; Morgan et al., 2015; Phillips et al., 2016; Wagner et al., 2013). Figure 6 shows the WINTER  $\gamma(\text{N}_2\text{O}_5)$  medians and distributions by flight, in comparison to those of factors thought to influence the rate-limiting uptake process, including RH, temperature, pH, and aerosol composition. A dependence of  $\gamma(\text{N}_2\text{O}_5)$  on any particular factor is not immediately clear in Figure 6. The relationships between  $\gamma(\text{N}_2\text{O}_5)$  and each individual factor are therefore individually presented in the following subsections to identify dominant factors associated with  $\gamma(\text{N}_2\text{O}_5)$  and provide insight into the uptake mechanism.

### 4.2.1. Ambient Temperature

Early laboratory studies reported a strong negative temperature dependence of  $\gamma(\text{N}_2\text{O}_5)$  (i.e., increasing with decreasing temperature) on highly acidic sulfuric acid particles (pH  $\sim -1$ ) (Hallquist et al., 2000; Robinson et al., 1997). In contrast, smaller and/or inconsistent trends with temperature have been observed on weakly acidic/neutral aerosol including  $(\text{NH}_4)_2\text{SO}_4$  and  $(\text{NH}_4)\text{HSO}_4$  below 290 K (Griffiths & Cox, 2009; Hallquist et al., 2003; Mozurkewich & Calvert, 1988), nitrate-containing aerosol at any temperature (Hallquist et al., 2003), pure water and 1 M NaCl from over 260–280 K (George et al., 1994; Schweitzer et al., 1998), and a single study of pure organic liquid particles over 268–298 K (Gross et al., 2009). A negative temperature dependence is consistent with uptake limitation by either mass accommodation (R1) ( $\alpha$ ) (a thermodynamic process governed by Gibb's free energy that becomes more favorable as lower temperatures reduce the entropic barrier to uptake, as discussed in Griffiths and Cox, 2009) or the net balance between bulk-phase solubility (R3) and reevaporation (R2) (as discussed in Mozurkewich and Calvert, 1988). Clear trends in previous studies, however, appear to be complicated by the presence of halides ( $\text{X}^-$ ), water, and the reversible reaction of  $\text{N}_2\text{O}_5$  through the nitrate effect (section 4.2.3), suggesting uptake is either limited by a different mechanistic step or that these steps are not dominantly controlled by temperature.

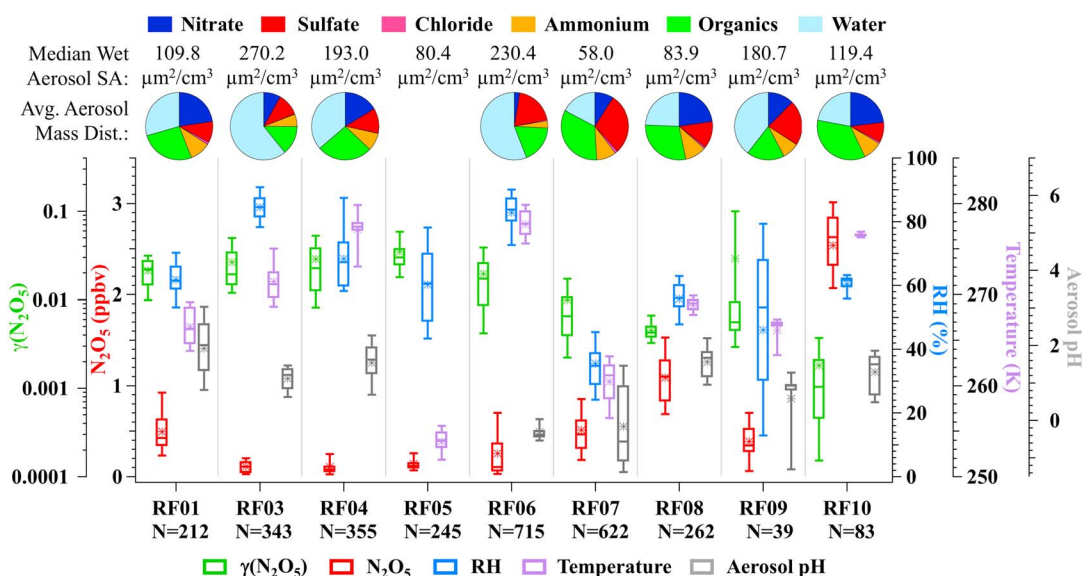


**Figure 6.** Model-derived  $\gamma(\text{N}_2\text{O}_5)$  and observed ambient variables listed by flight. Box and whisker plots show 10th–90th and 25th–75th percentiles, with median (bar) and average (star) values. Pie charts represent the average distribution of submicron aerosol composition as measured by the AMS with corresponding median surface area (including water) listed above. To account for the presence of sea salt, aerosol chloride was measured by the PILS-IC, with an average contribution ranging from 0.1 to 1.2% for all night flights. AMS measurements were unavailable on RF05 as well as subsequently calculated pH and liquid water. Data shown are only for points with simultaneous  $\gamma(\text{N}_2\text{O}_5)$  observations, the number of which are given under each flight label.

WINTER determinations of  $\gamma(\text{N}_2\text{O}_5)$  do not show a statistically significant ( $p > 0.05$ ) correlation with temperature over the observed range of 247–283 K (Figure 7). Despite a lack of trend and a high level of variability, the model-derived  $\gamma(\text{N}_2\text{O}_5)$  values largely fall within the range of previous laboratory determinations discussed above (Figure S25). Phillips et al. (2016) is the only previous field study to examine the temperature dependence of  $\gamma(\text{N}_2\text{O}_5)$  and also found no clear trend over the range ~278–292 K for particles containing mixtures of organics, sulfate, ammonium, and nitrate. Similar to past laboratory results, Figure 7 suggests that  $\gamma(\text{N}_2\text{O}_5)$  is not dominantly controlled by temperature.

#### 4.2.2. RH/Aerosol Liquid Water

Resistance to solubility (R3) and/or reaction (R5) will decrease with an increased availability of liquid water, consistent with previous laboratory results showing more efficient uptake on aqueous aerosol than on solid inorganic or organic particles (e.g., Gross et al., 2009; Hu & Abbatt, 1997; Mozurkewich & Calvert, 1988; Stewart et al., 2004; Thornton & Abbatt, 2005; Thornton et al., 2003). Aerosol liquid water is largely controlled by ambient RH and aerosol hygroscopicity, making aerosol water molarity a potentially better predictor of  $\gamma(\text{N}_2\text{O}_5)$  on ambient aerosol. Two previous laboratory studies found a positive dependence on water molarity (Badger et al., 2006; Thornton et al., 2003), but a larger number have presented  $\gamma(\text{N}_2\text{O}_5)$  as a function of RH. These studies show a positive trend in  $\gamma(\text{N}_2\text{O}_5)$  with RH on weakly acidic/neutral aerosol, but one that is composition dependent and becomes weaker as RH increases above 50% (Badger et al., 2006; Behnke et al., 1997; Bertram & Thornton, 2009; Folkers et al., 2003; Folkers, 2001; Hallquist et al., 2003; Kane et al., 2001; Mentel et al., 1999; Mozurkewich & Calvert, 1988; Sohn, 1998; Wahner, Mentel, Sohn, & Stier, 1998). The change in correlation strength with increasing RH suggests that uptake is limited by the term  $\Gamma_{\text{sol}} + \Gamma_{\text{rxn}}$  ((R3) and/or (R5)) at low RH, but becomes limited by a different process, such as  $\alpha$

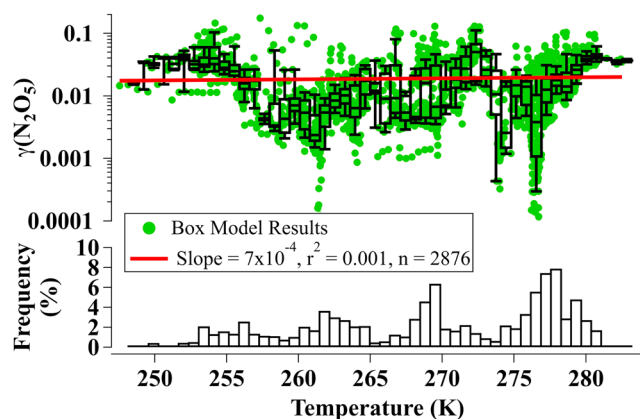


**Figure 7.** Variation of  $\gamma(\text{N}_2\text{O}_5)$  with ambient-observed temperature. Box and whisker plots show 10th to 90th (bars), and 25th to 75th (boxes) percentiles and median values. The histogram shows the distribution of observed temperatures. The red line shows the linear fit to all of the data points (green) with fit results listed in the box.



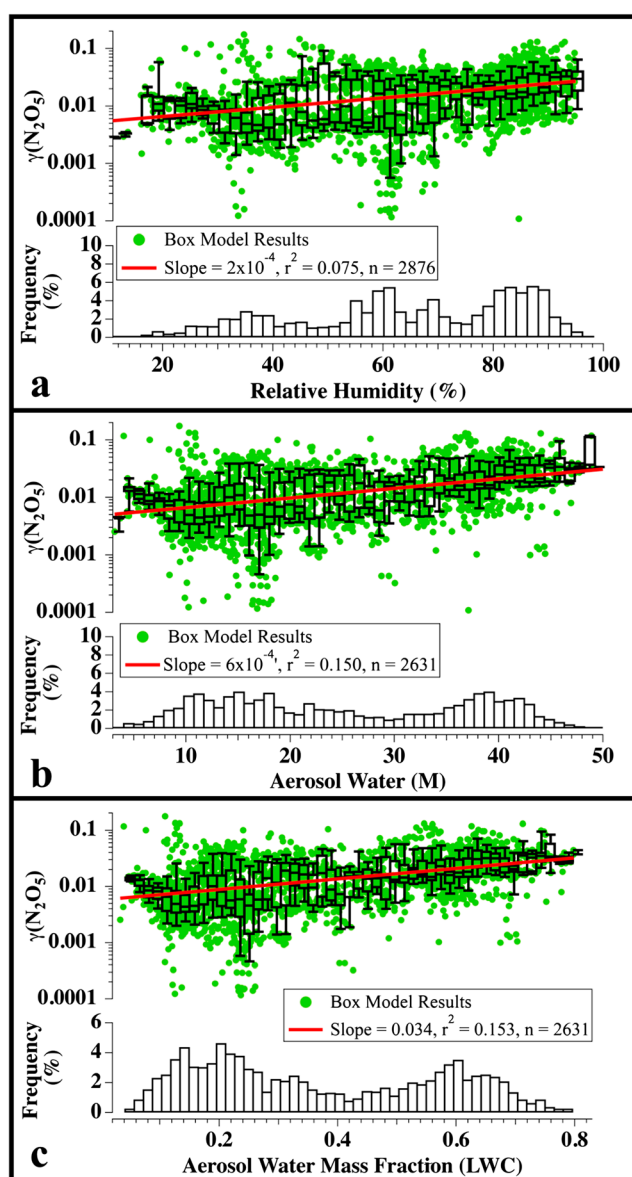


**Figure 8.** Variation in  $\gamma(\text{N}_2\text{O}_5)$  with (a) relative humidity, (b) aerosol water molarity (M), and (c) aerosol water liquid content (LWC) (i.e., water mass fraction). Box and whisker plots, histogram, and fit lines as in Figure 7.

(R1) as water availability increases (e.g., Bertram & Thornton, 2009; Thornton & Abbatt, 2005). The exact RH associated with this sensitivity change is thought to depend on the deliquescence point of each aerosol type and its propensity to form supersaturated liquids (e.g., Kane et al., 2001), which can be impacted by aerosol acidity and organics (e.g., Losey et al., 2016). In addition, several studies have observed the opposite, decreasing trend in  $\gamma(\text{N}_2\text{O}_5)$  with RH on highly acidic sulfuric acid particles (Fried et al., 1994; Hallquist et al., 2000; Hu & Abbatt, 1997; Kane et al., 2001; Mozurkewich & Calvert, 1988), which supports an alternative, acid-catalyzed mechanism discussed in section 4.2.5.

WINTER  $\gamma(\text{N}_2\text{O}_5)$  values show a statistically significant ( $p < 0.05$ ), positive correlation with aerosol water. For completeness, Figure 8 shows the correlations with RH (a), aerosol water molarity (b) and aerosol liquid water content (c). In this study aerosol water molarity and liquid water content (aerosol water mass fraction) are calculated using  $< 1 \mu\text{m}$  AMS aerosol measurements and estimates of aerosol liquid water and organic hygroscopicity, as described in section S1. The higher correlation observed with water molarity ( $r^2 = 0.150$ ) than with RH ( $r^2 = 0.075$ ) is consistent with uptake being limited by the availability of aerosol water, which is not always directly proportional to RH. There is not, however, a clear plateau above 50% RH or  $\sim 15 \text{ M}$   $[\text{H}_2\text{O}]$  as observed in previous laboratory studies (e.g., Bertram & Thornton, 2009), which suggests a more constant water dependence under all observed conditions. Despite the large variability in WINTER values in Figure 8, data above 20% RH roughly fall within the range of laboratory values for inorganic aerosol discussed above (Figure S26). No previous field studies have examined the  $\gamma(\text{N}_2\text{O}_5)$  dependence on aerosol water molarity, but several studies have observed a positive, though generally weak correlation with RH from both ground (Bertram, Thornton, Riedel, Middlebrook, et al., 2009; Brown et al., 2016; Phillips et al., 2016; X. Wang et al., 2017) and aircraft (Morgan et al., 2015) campaigns. No correlation with RH was observed over 34–85% for flights over Texas in October 2006 (Brown et al., 2009). High  $\gamma(\text{N}_2\text{O}_5)$  values in Beijing, however, were attributed to high aerosol liquid water content (H. Wang et al., 2017). Previous studies have not quantitatively assessed the trend in  $\gamma(\text{N}_2\text{O}_5)$  with liquid water content (water mass fraction), but the higher correlation in Figure 8 ( $r^2 = 0.153$ ) may suggest this as an even stronger predictor of  $\gamma(\text{N}_2\text{O}_5)$  than water molarity.

#### 4.2.3. The Nitrate Effect

Nonlinear suppression of  $\gamma(\text{N}_2\text{O}_5)$  by aerosol-phase nitrate, or the “nitrate effect,” has been consistently observed on both laboratory-derived (Bertram & Thornton, 2009; Hallquist et al., 2003; Mentel et al., 1999; Thornton et al., 2003; Wahner, Mentel, Sohn, & Stier, 1998) and ambient-observed nitrate-containing aerosol (Bertram, Thornton, Riedel, Middlebrook, et al., 2009; Morgan et al., 2015; Riedel et al., 2012; Wagner et al., 2013). WINTER  $\gamma(\text{N}_2\text{O}_5)$  values follow this expected trend and show a statistically significant ( $p < 0.05$ ) negative correlation with aerosol nitrate mass fraction (including water) in Figure 9a.

The current mechanism suggests that aerosol nitrate may impact the rate-limiting step,  $\Gamma_{\text{sol}} + \Gamma_{\text{rxn}}$ , but may also serve to reduce net  $\gamma(\text{N}_2\text{O}_5)$  in addition to, and independent from, the actual rate-limiting process. For example, suppression in net uptake has been observed in previous laboratory studies in which nitrate has caused additional reductions in  $\gamma(\text{N}_2\text{O}_5)$  under low RH where uptake is expected to be rate limited by the presence of aerosol water ((R3) or (R5)) (Bertram & Thornton, 2009). This observation has been explained with the chemical mechanism in Figure 2 as a competition between aerosol-phase nitrate ( $\text{NO}_3^-$ ) and  $\text{H}_2\text{O}$  for the  $\text{H}_2\text{ONO}_2^+$  intermediate, in which the recombination reaction with  $\text{NO}_3^-$  (R4) has a 20–30 times larger rate

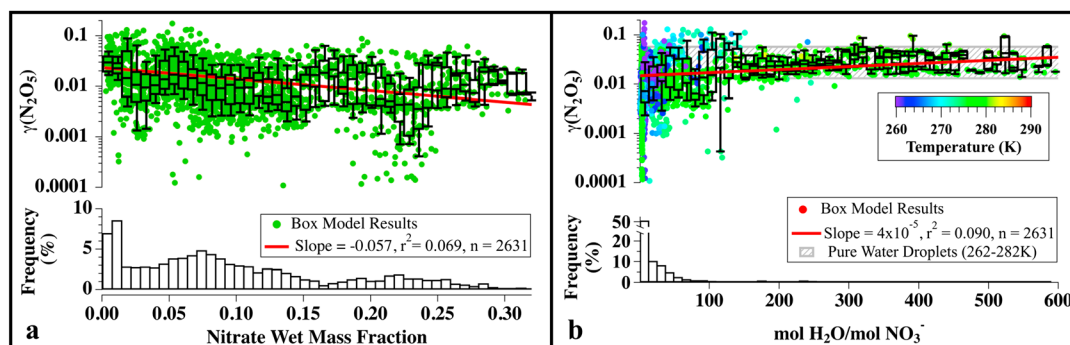


**Figure 9.** (a) Variation in  $\gamma(\text{N}_2\text{O}_5)$  with aerosol nitrate mass fraction, including contribution from aerosol water. (b) Variation in  $\gamma(\text{N}_2\text{O}_5)$  with aerosol  $\text{H}_2\text{O}:\text{NO}_3^-$  molar ratio, colored by ambient temperature. The shaded region represents the range of previous laboratory determinations of  $\gamma(\text{N}_2\text{O}_5)$  on pure water droplets over the range of 262–277 K (George et al., 1994), 264–275 K (Schweitzer et al., 1998), and 271–282 K (Van Doren et al., 1990). Box and whisker plots, histograms, and fit lines as in preceding figures.

constant than reaction with  $\text{H}_2\text{O}$  (R5) (Bertram & Thornton, 2009; Griffiths et al., 2009). Solvated  $\text{N}_2\text{O}_5$  will therefore reform at sufficiently low  $\text{H}_2\text{O}:\text{NO}_3^-$  molar ratios and evaporate back into the gas phase via (R2), resulting in apparent suppression of the observed net uptake coefficient, even when the overall process is limited by water availability (e.g., Bertram & Thornton, 2009; Mentel et al., 1999; Thornton et al., 2003; Wahner, Mentel, Sohn, & Stier, 1998). At high  $\text{H}_2\text{O}:\text{NO}_3^-$  ratios (dilute nitrate), however,  $\gamma(\text{N}_2\text{O}_5)$  can also become nitrate independent as the rate of (R5) exceeds that of (R4). The decrease in  $\gamma(\text{N}_2\text{O}_5)$  suppression with increasing  $\text{H}_2\text{O}:\text{NO}_3^-$  molar ratios has been observed in both laboratory studies (e.g., Bertram & Thornton, 2009; Griffiths et al., 2009; Mentel et al., 1999; Wahner, Mentel, Sohn, & Stier, 1998) and field observations (Morgan et al., 2015; Riedel et al., 2012; Wahner, Mentel, Sohn, & Stier, 1998), as well as in WINTER results, shown in Figure 9b.

Clear suppression of  $\gamma(\text{N}_2\text{O}_5)$  at low  $\text{H}_2\text{O}:\text{NO}_3^-$  ratios is obscured to some extent by scatter in the WINTER data. Even when normalized to values at high  $\text{H}_2\text{O}:\text{NO}_3^-$  ratios (not shown), persistent scatter in the WINTER data below 100  $\text{H}_2\text{O}:\text{NO}_3^-$  suggests that nitrate suppression is not the only factor controlling uptake. There is agreement, however, in the magnitude of  $\gamma(\text{N}_2\text{O}_5)$  at the highest molar ratios ( $> 100$ ) where WINTER  $\gamma(\text{N}_2\text{O}_5)$  values become nitrate independent and fall within the range of pure water (shaded region of Figure 9b) (George et al., 1994; Schweitzer et al., 1998; Van Doren et al., 1990). Bertram and Thornton (2009) observed a similar plateau in  $\gamma(\text{N}_2\text{O}_5)$  to a value of 0.03 at  $\text{H}_2\text{O}:\text{NO}_3^-$  ratios  $> 40$ , while Morgan et al. (2015) and Riedel et al. (2012) observed plateaus in field observations at  $\text{H}_2\text{O}:\text{NO}_3^-$  molar ratios  $> 50$ . Phillips et al. (2016) did not observe this trend over the range of ratios 0.5–60 in field data collected from a ground site in Germany. Though a clear plateau in WINTER  $\gamma(\text{N}_2\text{O}_5)$  values did not appear until a higher molar ratio ( $\sim 100$ ), qualitative similarities between WINTER results and previous studies suggest that conditions exist on ambient aerosol where  $\gamma(\text{N}_2\text{O}_5)$  is not suppressed by nitrate and falls within a limited range of values consistent with laboratory studies of uptake to liquid water. These data, however, account for a small fraction ( $< 18\%$ ) of the total  $\gamma(\text{N}_2\text{O}_5)$  determinations during WINTER (two flights, RF03 and RF06, where thermodynamic partitioning and high humidity over the ocean contributed to  $\text{NO}_3^-$  dilution), suggesting that nitrate suppression must generally be considered for accurate uptake parameterization, even if uptake is rate limited by a different process.

#### 4.2.4. Aerosol Nitrate/Chloride

Similar to aerosol-phase  $\text{NO}_3^-$ , particle chloride ( $\text{Cl}^-$ ) is expected to influence  $\gamma(\text{N}_2\text{O}_5)$  without necessarily contributing to the rate-limiting step. This occurs through a reduction in nitrate suppression by a competition between  $\text{NO}_3^-$  and  $\text{Cl}^-$  for the  $\text{H}_2\text{ONO}_2^+$  intermediate, in which the reaction rate constant with  $\text{Cl}^-$  (R6) is  $\sim 30$  times greater than the rate constant for  $\text{NO}_3^-$  (R4) (Bertram & Thornton, 2009). Previous laboratory studies have found efficient uptake onto chloride-containing aerosol (Behnke et al., 1991; Behnke et al., 1997; McNeill et al., 2006; Stewart et al., 2004; Thornton & Abbatt, 2005) with Bertram and Thornton (2009) observing complete elimination of the nitrate effect for mixed aqueous  $\text{NaNO}_3/\text{NaCl}$  particles above 2 M aerosol  $\text{Cl}^-$  ( $[\text{Cl}^-]$ ).

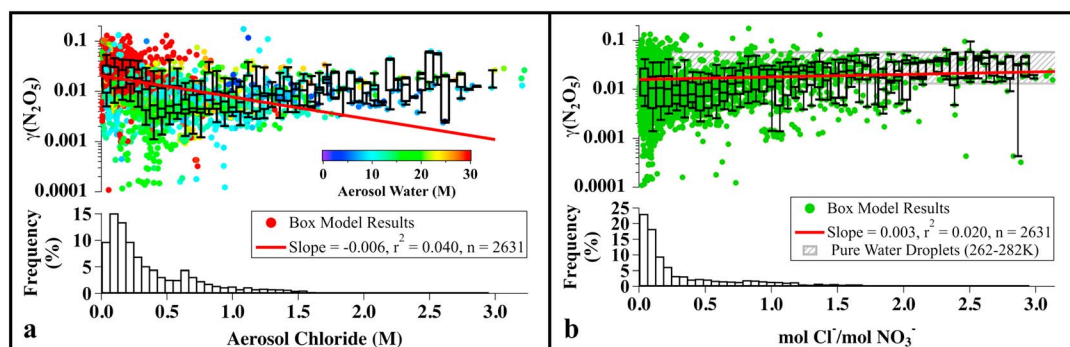


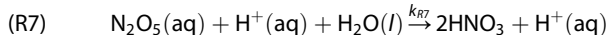
**Figure 10.** (a) Variation in  $\gamma(\text{N}_2\text{O}_5)$  with aerosol chloride molarity (derived from PILS-IC measurements), colored by aerosol water molarity. (b) Variation in  $\gamma(\text{N}_2\text{O}_5)$  with aerosol  $\text{Cl}^-:\text{NO}_3^-$  molar ratio. The gray shaded region represents the range of previous laboratory determinations of  $\gamma(\text{N}_2\text{O}_5)$  on pure water droplets. Box and whisker plots, histograms, and fit lines as in preceding figures.

Results for WINTER are shown in Figure 10 as a function of  $[\text{Cl}^-]$  (a) and  $\text{Cl}^-:\text{NO}_3^-$  molar ratio (b). WINTER data in Figure 10a do not show a positive correlation between  $\gamma(\text{N}_2\text{O}_5)$  and  $[\text{Cl}^-]$  (as measured by the particle-into-liquid sampler, PILS-IC). As expected, however, Figure 10b shows a statistically significant ( $p < 0.05$ ) positive correlation with  $\text{Cl}^-:\text{NO}_3^-$  ratio, but with large scatter in the data at the lowest ratios. A plateau in  $\gamma(\text{N}_2\text{O}_5)$  values was also observed at the highest molar ratios, similar to the trend observed by Bertram and Thornton (2009), but these high  $\text{Cl}^-:\text{NO}_3^-$  ratios were only seen in a small fraction of WINTER data. A previous field study by Morgan et al. (2015) found only a weak dependence of  $\gamma(\text{N}_2\text{O}_5)$  on aerosol chloride mass fraction and did not evaluate the trend with  $[\text{Cl}^-]$  or  $\text{Cl}^-:\text{NO}_3^-$ . Overall, WINTER and previous field results suggest that aerosol  $\text{Cl}^-$  may influence  $\gamma(\text{N}_2\text{O}_5)$ , but that it is not a dominant predictor. The effects of aerosol  $\text{Cl}^-$  on various  $\gamma(\text{N}_2\text{O}_5)$  parameterizations are discussed in section 4.3.2.

#### 4.2.5. Aerosol pH

Previous laboratory studies of  $\text{N}_2\text{O}_5$  uptake onto highly acidic sulfuric acid surfaces found relatively large  $\gamma(\text{N}_2\text{O}_5)$  values with no dependence on RH at low humidity (Fried et al., 1994; Hallquist et al., 2000; Hu & Abbatt, 1997; Kane et al., 2001; Mozurkewich & Calvert, 1988; Robinson et al., 1997). These results led to an alternative mechanism first proposed by Robinson et al. (1997), in which  $\text{N}_2\text{O}_5$  solvation is catalyzed by the  $\text{H}^+$  ion instead of reaction with water. This reaction replaces (R3) and (R5) with the process shown in (R7). Though many of these previous laboratory studies were focused on highly acidic stratospherically

relevant  $\text{H}_2\text{SO}_4$  concentrations, some studies (e.g., Hallquist et al., 2000) observed enhanced uptake at lower, tropospherically relevant concentrations ( $\text{pH} \sim 1$ ), within the range observed during WINTER ( $\text{pH} -2$  to 5).



This analysis is the first field study to quantitatively examine the correlation between pH and  $\gamma(\text{N}_2\text{O}_5)$ . WINTER  $\gamma(\text{N}_2\text{O}_5)$  values have an overall negative correlation with pH ( $p < 0.05$ ), as would be expected according to (R7) (Figure 11). Acid-catalyzed hydrolysis, however, cannot be confirmed from WINTER data due to covariance of pH with aerosol water and  $\text{NO}_3^-$ . As shown in Figure S27, pH is correlated with aerosol nitrate above pH 1 due to thermodynamic partitioning that leads to an increase in aerosol nitrate with decreasing acidity. One previous field study has suggested this thermodynamic partitioning as a potential explanation for variations in  $\gamma(\text{N}_2\text{O}_5)$  over the eastern United States (Brown et al., 2006). To account for the possibility of nitrate partitioning driving the overall negative trend, data in Figure 11 were additionally fit

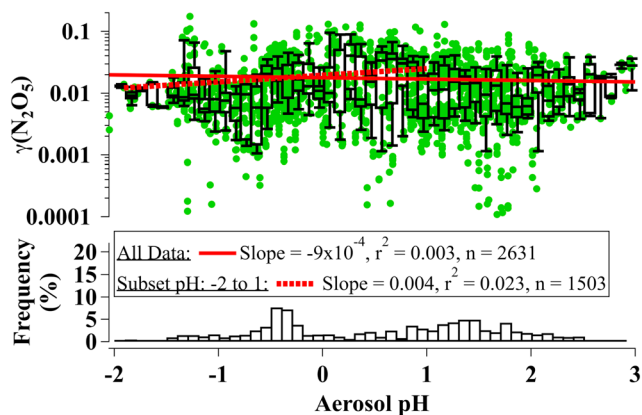


**Figure 11.** Variation in  $\gamma(\text{N}_2\text{O}_5)$  with aerosol pH. Box and whisker plot, histogram, and fit line as in preceding figures. Dashed line is the linear fit to data between pH  $-2$  and  $1$  to separate the influence from nitrate suppression at  $\text{pH} > 1$ .

between pH  $-2$  and  $1$  (dashed line), yielding a statistically significant ( $p < 0.05$ ) positive correlation, opposite of the expected trend. This result suggests that despite the high particle acidity observed during WINTER (Guo et al., 2016), acid catalysis does not dominantly contribute to  $\gamma(\text{N}_2\text{O}_5)$ .

#### 4.2.6. Aerosol Organic Content

While one recent study has shown that cationic surfactants can enhance the rate of  $\text{N}_2\text{O}_5$  bulk-phase reaction by facilitating surface reactions (Shaloski et al., 2017), the majority of previous laboratory studies have found that the presence of organics suppresses  $\gamma(\text{N}_2\text{O}_5)$  relative to pure inorganic salts. The magnitude of suppression, however, is strongly dependent on the organic composition (e.g., Griffiths et al., 2009; Gross et al., 2009), particle phase state (e.g., Thornton et al., 2003), and the presence of surfactants (e.g., Cosman et al., 2008, and references therein), which are controlled by factors such as RH, temperature, and molecular structure and composition. The mechanism by which organic suppression occurs can be explained as a limitation to  $\alpha$ ,  $\Gamma_{\text{sol}}$ , and/or  $\Gamma_{\text{rxn}}$ , which are difficult to deconvolve. For example, insoluble organic surfactants can create monolayers or liquid-liquid phase separations (You et al., 2014, and references therein) that either limit the exchange of  $\text{N}_2\text{O}_5$  across the air-surface interface (R1:  $\alpha$ ) or reduce  $\text{N}_2\text{O}_5$  bulk-phase solubility and/or diffusion and reaction ((R3)–(R6):  $\Gamma_{\text{sol}}$  and/or  $\Gamma_{\text{rxn}}$ ) (Badger et al., 2006; Cosman et al., 2008; Folkers et al., 2003; McNeill et al., 2006; Thornton & Abbatt, 2005). Organic-induced phase changes from aqueous to glassy (highly viscous) solids can also occur as a function of  $T$ , RH, and molecular composition (Shiraiwa et al., 2017), limiting the amount of available surface water for  $\text{N}_2\text{O}_5$  solvation and reaction ((R3) and (R5):  $\Gamma_{\text{sol}}$  and/or  $\Gamma_{\text{rxn}}$ ). Various  $\gamma(\text{N}_2\text{O}_5)$  parameterizations have attempted to account for these suppressive effects by incorporating increased resistance in (E5) from both reactive and nonreactive organic coatings that impact  $\text{N}_2\text{O}_5$  solubility and diffusion (e.g., Anttila et al., 2006; Gaston et al., 2014), or by parameterizing  $\alpha$  as a function of organic mass fraction and RH (Badger et al., 2006). These and other parameterizations for organics are discussed further in section 4.3.2.

Although aerosol organics are known to suppress  $\gamma(\text{N}_2\text{O}_5)$ , composition-driven changes in morphology (i.e., liquid organic coatings) and/or phase state are difficult to predict with available WINTER aerosol observations. Similarly, organic composition and morphology are unknown factors in previous field studies of  $\gamma(\text{N}_2\text{O}_5)$ , though one study, using  $\gamma(\text{N}_2\text{O}_5)$  from Riedel et al. (2012) and single particle measurements from an aerosol time-of-flight mass spectrometer, concluded that molecular composition and physical properties of the aerosol organics were likely the largest controlling factors during that study (Ryder et al., 2014).

Laboratory studies indicate that organic coatings and/or liquid-liquid phase separations should result in a negative correlation of  $\gamma(\text{N}_2\text{O}_5)$  with organic dry mass fraction (McNeill et al., 2006) and positive correlation with atomic O:C ratio (e.g., Bertram et al., 2011; Gaston et al., 2014). WINTER data have statistically significant ( $p < 0.05$ ) correlations with these variables with slopes of the predicted sign (Figures 12a and 12d) but with low correlation coefficients ( $r^2 < 0.02$ ) relative to other variables (Table 3). A stronger ( $r^2 = 0.114$ ), negative correlation with organic mass fraction is found when aerosol water is included in the total mass (Figure 12b). This observation suggests that the magnitude of organic suppression could be impacted by the presence of water, which could have implications for how the organic suppression is treated in parameterizations. This observation also agrees with previous studies that observed reductions in organic suppression at high RH on aqueous organics or partially coated aerosol (e.g., Badger et al., 2006; Thornton et al., 2003). With dry organic mass fraction, previous field results have shown either weak ( $r^2 = 0.004$ ) or no correlation with  $\gamma(\text{N}_2\text{O}_5)$  (Brown et al., 2009; Morgan et al., 2015) and have not assessed the relative relationship with wet mass fraction. The only other field study to evaluate  $\gamma(\text{N}_2\text{O}_5)$  as a function of the O:C ratio observed no trend over the relatively small range of 0.49 to 0.66 (Morgan et al., 2015). Restricting the fit to WINTER data with O:C between 0.5 and 1 (similar to that in Gaston et al., 2014) increased the correlation coefficient to 0.063. Two previous summertime field studies have additionally used the  $\text{Org}:\text{SO}_4^{2-}$  ratio as a proxy for the amount of organics relative to surface water (due to  $\text{SO}_4^{2-}$  hygroscopicity). These studies observed cases in which there was both strong negative (Bertram, Thornton, Riedel, Middlebrook, et al., 2009) and no observable dependences (Bertram, Thornton, Riedel, Middlebrook, et al., 2009; Phillips et al., 2016) on this ratio, likely the result of differences in aerosol composition and water content. The weak correlation with this factor in Figure 12c suggests that the  $\text{Org}:\text{SO}_4^{2-}$  is not a strong predictor of  $\gamma(\text{N}_2\text{O}_5)$  during WINTER compared to other variables but may also reflect the generally lower concentrations of aerosol  $\text{SO}_4^{2-}$  relative to  $\text{NO}_3^-$  during the winter season.



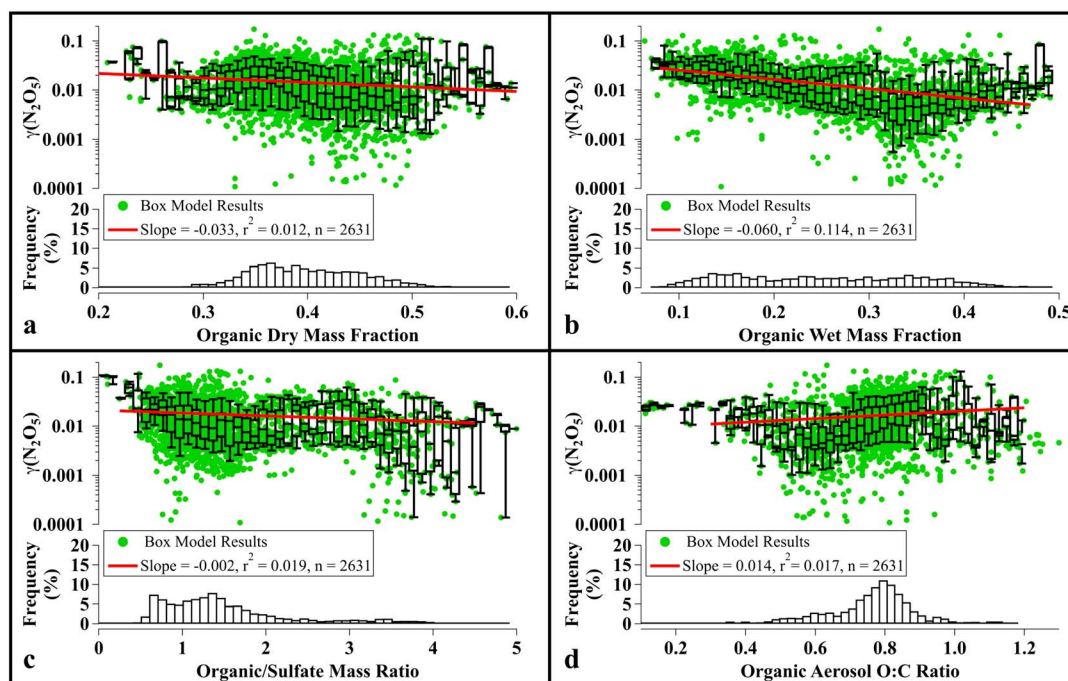


**Figure 12.** Variation in  $\gamma(\text{N}_2\text{O}_5)$  with (a) aerosol organic dry mass fraction, (b), organic wet mass fraction (including water), (c) aerosol Org: $\text{SO}_4^{2-}$  mass ratio, and (d) O:C ratio. All aerosol data were collected by the AMS. Box and whisker plots, histograms, and fit lines as in preceding figures.

Overall, many of the  $\gamma(\text{N}_2\text{O}_5)$  WINTER values were lower than those predicted for uptake onto pure inorganic salts, especially at high humidity (e.g., Figure S26), suggesting some level of organic suppression. WINTER data, however, cannot confirm the magnitude nor the mechanism of this effect without knowledge or measurement of aerosol morphology (i.e., coatings) or phase due to concurrent impacts on  $\gamma(\text{N}_2\text{O}_5)$  from covarying factors, such as aerosol water and anions.

#### 4.2.7. Aerosol Size

Assuming dependence on a rate-limiting step, current theory suggests that  $\gamma(\text{N}_2\text{O}_5)$  will be dependent on aerosol size if reaction of the intermediate  $\text{H}_2\text{ONO}_2^+$  ((R4)–(R6)) occurs within the entire aerosol volume, but size independent if reaction occurs within the surface layer. These cases will have different implications for the parameterization of  $\gamma(\text{N}_2\text{O}_5)$  as the former suggests an aerosol size dependence, while the latter suggests a dependence on aerosol surface composition and morphology. Volume or surface layer reaction can be estimated by the reacto-diffusion length (diffusion distance of  $\text{N}_2\text{O}_5$  prior to bulk-phase reaction,  $q$  [m]), which has been shown by one study to vary enough that uptake can be volume-limited on sulfate aerosol while surface-limited on sodium chloride (Gaston & Thornton, 2016). Other laboratory studies on both inorganic and organic aerosol have been inconclusive, showing evidence for both surface and volume-limited reactions (e.g., Mozurkewich & Calvert, 1988). As discussed by Thornton et al. (2003) and Gaston and Thornton (2016), volume-limited reactions should yield a linear, positive correlation between  $\gamma(\text{N}_2\text{O}_5)$  and aerosol size (SA-weighted particle radius or volume to SA concentration ratio) with a slope indicative of the reaction rate between  $\text{N}_2\text{O}_5$  and water, anions, or halides ((R4)–(R6)). WINTER  $\gamma(\text{N}_2\text{O}_5)$  results (not shown) are consistent with this positive trend over the observed range (30–300 nm) of median SA-weighted particle radii (defined in section S6) but have a low correlation coefficient ( $r^2 = 0.025$ ), suggesting that aerosol size is an overall weak predictor of  $\gamma(\text{N}_2\text{O}_5)$  relative to other factors, such as aerosol water. These results add to the inconclusiveness of prior studies but likely represent the varying, overlapping size dependences (or independences) of different aerosol compositions, indicating that factors other than aerosol size are stronger predictors of  $\gamma(\text{N}_2\text{O}_5)$  on ambient aerosol.

#### 4.2.8. Trends Summary

Identification of the rate-limiting process in equation (E5) and its associated factors are important for accurate parameterization of  $\gamma(\text{N}_2\text{O}_5)$ . Correlations between WINTER  $\gamma(\text{N}_2\text{O}_5)$  results and all uptake-relevant variables



**Table 3**  
Summary of  $\gamma(\text{N}_2\text{O}_5)$  Trend Analyses

	Variable	Correlation coefficient ( $r^2$ )	Correlation sign	N
1	Aerosol liquid water content (mass fraction)	0.153	+	2631
2	Aerosol water molarity	0.150	+	2631
3	Aerosol organic wet mass fraction	0.114	—	2631
4	Aerosol $\text{H}_2\text{O}:\text{NO}_3^-$ molar ratio	0.090	+	2631
5	Ambient RH	0.075	+	2876
6	Aerosol nitrate wet mass fraction	0.069	—	2631
7	Aerosol O:C ratio (0.5–1)	0.063	+	2372
8	Aerosol chloride wet mass fraction	0.039	—	2631
9	Aerosol nitrate dry mass fraction	0.032	—	2631
10	Surface area weighted aerosol radius	0.025	+	2876
11	Aerosol pH (–2 to 1)	0.023	+	1503
12	Aerosol $\text{Cl}^-:\text{NO}_3^-$ molar ratio	0.020	+	2631
13	Aerosol organic:sulfate mass ratio	0.019	—	2631
14	Aerosol O:C ratio (full range)	0.017	+	2631
15	Aerosol chloride dry mass fraction	0.013	—	2631
16	Aerosol organic dry mass fraction	0.012	—	2631
17	Aerosol pH (full range)	0.003	—	2631
18	Ambient temperature	0.001 <sup>a</sup>	+	2876

<sup>a</sup>Not a statistically significant result ( $p > 0.05$ ).

(summarized in Table 3) show some of the strongest correlations with aerosol water and nitrate, suggesting that uptake (assuming the currently accepted mechanism) is largely controlled by  $\Gamma_{\text{sol}} + \Gamma_{\text{rxn}}$  and more specifically, impacted by the  $\text{N}_2\text{O}_5$  solvation reaction (R3) ( $\text{N}_2\text{O}_5 + \text{H}_2\text{O}$ ) and/or bulk-phase reactions (R5) and (R4) ( $\text{H}_2\text{ONO}_2^+ + \text{H}_2\text{O}$  or  $\text{NO}_3^-$ ). Uptake suppression from aerosol organics is also likely, due to the third highest correlation with wet organic mass fraction and generally lower  $\gamma(\text{N}_2\text{O}_5)$  values during WINTER than those derived on pure inorganic laboratory aerosol. Correlations, however, between  $\gamma(\text{N}_2\text{O}_5)$  and aerosol organic mass fraction, O:C ratio, and  $\text{Org}:\text{SO}_4^{2-}$  cannot discriminate as to whether an organic suppression occurs by impacting  $\alpha$  and/or  $\Gamma_{\text{sol}} + \Gamma_{\text{rxn}}$ . In addition, the observed positive correlation between  $\gamma(\text{N}_2\text{O}_5)$  and the most highly acidic aerosols (pH –2 to 1) does not support the importance of an acid-catalyzed mechanism.

The results presented here are generally consistent with those observed in previous laboratory and field studies (when trends have been reported). Despite this general agreement, low correlation ( $r^2 = 0.153$ ) of the most highly correlated variable (liquid water content) suggests that uptake is either sensitive to nonmeasured variables (such as aerosol morphology (i.e., liquid organic coating) or phase) or to a large number of interrelated variables (Table S7), highlighting the difficulty in identifying the dominant controlling factors required to develop a robust parameterization. The final section uses these results in combination with several parameterizations previously/currently implemented in 3-D models to evaluate their applicability to WINTER conditions and to provide insight for improving the predictive capabilities of  $\gamma(\text{N}_2\text{O}_5)$  during winter over the eastern United States, where  $\gamma(\text{N}_2\text{O}_5)$  is seasonally important.

### 4.3. Parameterization of $\gamma(\text{N}_2\text{O}_5)$

#### 4.3.1. Previous $\gamma(\text{N}_2\text{O}_5)$ Parameterizations

When first incorporated into 3-D chemical transport models,  $\gamma(\text{N}_2\text{O}_5)$  was set to a constant value of 0.1 for sulfate-containing aerosol, broadly considered at that time as a proxy for tropospheric aerosol, based on early laboratory measurements of uptake onto water, ammonium bisulfate, and sulfuric acid particles (Dentener & Crutzen, 1993). As reviewed by Chang et al. (2011), later laboratory studies suggested that uptake onto tropospherically relevant aerosol was composition dependent and much less efficient, leading Evans and Jacob (2005) to develop a parameterization (hereafter referred to as EJ05) based on the work of Kane et al. (2001), Hallquist et al. (2003), and Thornton et al. (2003) to capture the temperature and RH dependence of  $\gamma(\text{N}_2\text{O}_5)$  onto externally mixed inorganic salts and suppression by pure organic liquids. At the time, incorporation of EJ05 into GEOS-Chem improved model predictions of climatological observations (Evans & Jacob,

2005). Since then, the inorganic component of EJ05 has been largely replaced by a parameterization by Bertram and Thornton (2009) (hereafter BT09) expanded from earlier work (Mentel et al., 1999; Wahner, Mentel, Sohn, & Stier, 1998), which accounts for the water, nitrate, and chloride effects on internally mixed aerosol through the dependence of  $\gamma(\text{N}_2\text{O}_5)$  on aerosol water, size, and molar ratios of  $\text{H}_2\text{O}:\text{NO}_3^-$  and  $\text{Cl}^-:\text{NO}_3^-$ . Davis et al. (2008) (Dav08) additionally used a statistical analysis of early laboratory studies (similar to those used by Evans and Jacob, 2005) to develop a parameterization for internally mixed inorganic aerosol as a function of RH and temperature for different sulfate- and nitrate-containing particles. Neither Dav08 nor BT09 directly includes a dependence on aerosol organics, though BT09 can account for organic-associated changes in aerosol water. Both require combination with additional organic parameterizations, such as those described in Anttila et al. (2006), to calculate total  $\text{N}_2\text{O}_5$  loss rates impacted by surface-organic impedance. These current organic parameterizations, however, have large uncertainties in their mechanistic treatment (section 4.2.6) and have generally underpredicted  $\gamma(\text{N}_2\text{O}_5)$  in comparison to field studies (Brown et al., 2009; Morgan et al., 2015; Phillips et al., 2016). This uncertainty has led some models, such as the U.S. Environmental Protection Agency's Community Multiscale Air Quality Modeling System model, to exclude all organic dependencies in their parameterizations and simply note that  $\gamma(\text{N}_2\text{O}_5)$  may be overpredicted under high organic aerosol concentrations (Sarwar et al., 2014). To date, a single parametrization to account for the combined influence of all inorganic and organic aerosol components has not been developed. In the remaining sections, 14 previous and current versions of proposed and implemented parameterizations are compared to WINTER box model data to evaluate their applicability and provide insight for the development of the first field-based empirical  $\gamma(\text{N}_2\text{O}_5)$  parameterization.

#### 4.3.2. Comparison of Box Model Results to Laboratory-Derived Parameterizations

Nearly all laboratory-derived parameterizations for  $\gamma(\text{N}_2\text{O}_5)$  (except for IUPAC speciated recommendations and those for surface and volume confined uptake in Mentel et al., 1999 and Wahner, Mentel, Sohn, and Stier, 1998) are shown in comparison to WINTER box model results in Figures 13, 14, and S28. Details of each parameterization are given in Table S8 in section S6. Agreement between parameterized  $\gamma(\text{N}_2\text{O}_5)$  and box model results is assessed here according to the root-mean-square error (RMSE: standard deviation of the residuals) and by the median percent difference of each comparison (shown in Figure 14). The correlation coefficient ( $r^2$ ) and point number of each comparison are provided for reference in Figures 13, S28, and Table S8. Black squares in Figures 13 and S28 represent the median value of each parameterization relative to the WINTER median. Dashed lines in Figures 13 and S28 represent agreement within factors of  $\pm 2$  and  $\pm 10$  and are included as an additional evaluation method.

The original parameterization proposed by EJ05 generally overpredicts  $\gamma(\text{N}_2\text{O}_5)$  relative to the WINTER box model (Figure 13a), with a median percent difference of +120% (Figure 14). This result is consistent with two other field studies that found EJ05 to overpredict  $\gamma(\text{N}_2\text{O}_5)$  relative to values derived from the steady state approximation (Brown et al., 2009) and flow tube experiments (Bertram, Thornton, Riedel, Middlebrook, et al., 2009). EJ05 includes an RH and T dependence for  $\gamma(\text{N}_2\text{O}_5)$  onto sulfate aerosol as well as an RH dependence for organics, but may underpredict any organic suppression since it is based on laboratory data of water soluble organics (Thornton et al., 2003).

Three parameterizations shown in Figures 13b–13d consider uptake onto inorganic aerosol only. These parameterizations include the previously described Dav08 (Figure 13b) and BT09 (Figure 13d), as well as Rie03 (Figure 13c), developed by Riemer et al. (2003) to account for the increase in aerosol hygroscopicity associated with aerosol sulfate. All three parameterizations generally overpredicted WINTER results (Figure 14) with Rie03 producing the lowest RMSE (0.0172) and best median agreement (+9%), while BT09 had a slightly higher correlation coefficient ( $r^2 = 0.08$  versus 0.04). The underprediction of largest values by Rie03 is likely due to an imposed maximum value of 0.02 (value of pure water), smaller than the top 34% of WINTER values. Overprediction of smallest  $\gamma(\text{N}_2\text{O}_5)$  values by all three parameterizations is likely due to a missing organic suppression effect. Previous flights over the UK found that Rie03 underpredicted  $\gamma(\text{N}_2\text{O}_5)$  (Morgan et al., 2015), while flights over Texas found a general overprediction (Brown et al., 2009). The only three studies to compare Dav08 to field-derived data have also found large overpredictions by this parameterization (Bertram, Thornton, Riedel, Middlebrook, et al., 2009; Brown et al., 2009; Chang et al., 2016), but also a slight underprediction at low (< 30%) ambient RH (Chang et al., 2016). An additional version of Dav08 (Dav08B presented in the appendix of Davis et al., 2008) produced a lower RMSE than the original version (0.0243 versus 0.0320).

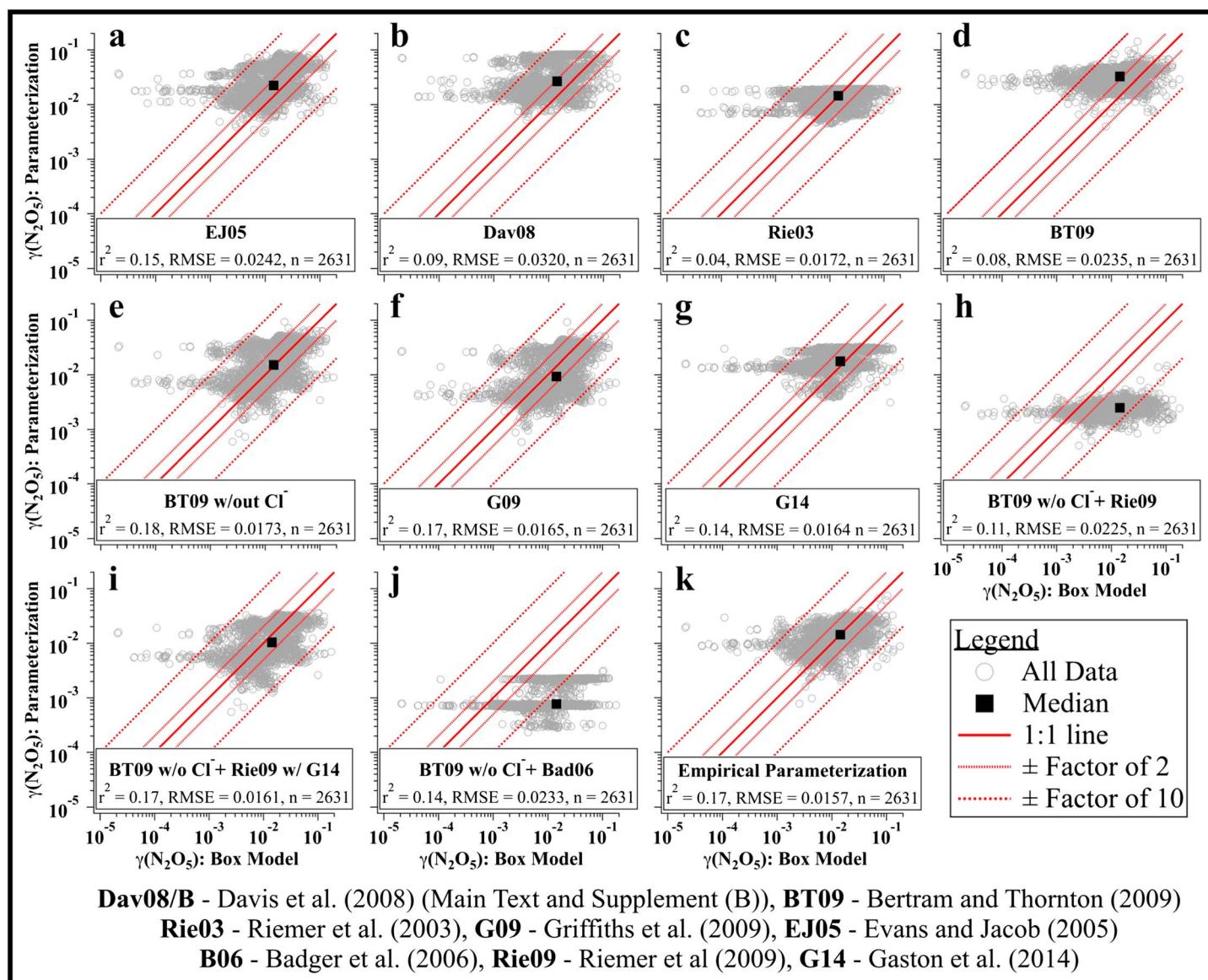
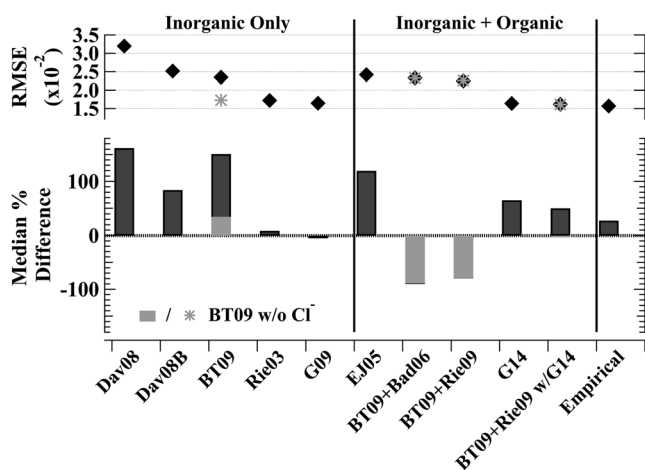


**Figure 13.** Comparisons between parameterized and model-derived  $\gamma(\text{N}_2\text{O}_5)$  values. Correlation coefficient, root-mean-square error, and point number are provided on each plot. Solid lines indicate the 1:1 line. Black squares represent median values. Dashed lines represent the range of values within factors of  $\pm 2$  and  $\pm 10$ .

when compared to WINTER data (Figure S28a), but one that remained higher than that for both BT09 (0.0235) and Rie03. For BT09, previous field studies have found both good agreement (Bertram & Thornton, 2009; Phillips et al., 2016) as well as overpredictions (Chang et al., 2016; Morgan et al., 2015; Riedel et al., 2012) of  $\gamma(\text{N}_2\text{O}_5)$ . Similar to results presented in Riedel et al. (2012) and Morgan et al. (2015), agreement with BT09 improved (higher  $r^2$  and lower RMSE) when the chloride contribution was removed from the parameterization (Figure 13e). A fourth parameterization (G09) in the same form as BT09 without  $\text{Cl}^-$ , but with different reaction rate constants (Griffiths et al., 2009), resulted in the lowest RMSE and median percent difference of all tested inorganic-only parameterizations (Figures 13, 14, and S28). These results suggest that (1) the reversal of the nitrate effect by chloride is not as large on ambient aerosol as on laboratory particles (i.e.,  $k_{R6}$  is too large,  $k_{R4}$  is too small, and/or aerosol chloride is unavailable for reaction with  $\text{H}_2\text{ONO}_2^+$ ) and/or (2) the suppressive effects of organics, which are not included in BT09, are better captured without an enhancement from chloride. All parameterizations, however, largely overpredict the smallest WINTER values, suggesting a missing suppressive effect.



Dav08/B - Davis et al. (2008) (Main Text and Supplement (B)), BT09 - Bertram and Thornton (2009)  
Rie03 - Riemer et al. (2003), G09 - Griffiths et al. (2009), EJ05 - Evans and Jacob (2005)  
B06 - Badger et al. (2006), Rie09 - Riemer et al. (2009), G14 - Gaston et al. (2014)

**Figure 14.** Comparison of 14 literature and empirical parameterizations relative to box model results. Comparisons are given in terms of their root-mean-square error (RMSE) (upper panel) and median percent difference (lower panel). Comparisons are listed in order of decreasing RMSE within each group of parameterization type (inorganic only, combined inorganic and organic, and empirical). Parameterizations that incorporated BT09 are shown with (dark gray) and without (light gray) the contribution from chloride.

Four additional parameterizations shown in Figures 13g–13j account for both the inorganic and organic aerosol components. The first (Figure 13g) follows the work of Anttila et al. (2006) and Gaston et al. (2014) and implements a full resistor model framework that models  $\text{N}_2\text{O}_5$  through a thick (reactive toward  $\text{N}_2\text{O}_5$ ) organic coating relative to the aqueous core (section S6). This method requires information about the rate constants of  $\text{N}_2\text{O}_5$  with the organic coating ( $k_{\text{org}}$ ) and aqueous core ( $k_{\text{aq}}$ ), reacto-diffusion parameters ( $q_{\text{org}}$  and  $q_{\text{aq}}$ ), and solubility and diffusion constants ( $H_{\text{org}}$  and  $D_{\text{org}}$ ) that were all adopted here from those presented in Gaston et al. (2014) as a function of O:C ratio and RH (Table S8). The second and third parameterizations follow the work of Riemer et al. (2009) and implement a simplified resistor framework that models uptake through a thin, nonreactive organic coating. As described in section S6 (and Table S8), this method does not require knowledge of  $k_{\text{org}}$  and combines an organic term described in Anttila et al. (2006) with BT09 (with and without  $\text{Cl}^-$ ). Bulk-phase solubility and diffusion coefficients were estimated in the first of these parameterizations (Figure 13h) by scaling the product  $H_{\text{aq}} * D_{\text{aq}}$  by a constant factor of  $\varepsilon = 0.03$  (Anttila et al., 2006; Riemer et al., 2009), which in the second (Figure 13i) was calculated as a function of RH and O:C ratio following Gaston et al. (2014). The final comparison (Figure 13j) does not assume an organic coating but rather applies a reduction to the mass accommodation coefficient ( $\alpha$ ) as a function of RH and dry organic mass fraction as described in Badger et al. (2006) (B06). Of these four approaches, parameterizing  $\alpha$  largely underpredicts  $\gamma(\text{N}_2\text{O}_5)$ , with a

median percent difference of (–89%) and the highest RMSE (Figure 14). Treating organics as a coating with the other three parameterizations improves the median percent difference but cannot reproduce the full range in WINTER values. Both underprediction and overprediction could result from a number of factors including incorrect estimation of the coating thickness, bulk-phase diffusion and solubility rates, or an enhancement from organics by facilitating surface reactions (Shaloski et al., 2017). Similar to WINTER, results from three previous field studies found that the simplified resistor framework generally underpredicted  $\gamma(\text{N}_2\text{O}_5)$ , likely due to an overprediction of the organic suppression effect (Morgan et al., 2015; Phillips et al., 2016), but improved agreement relative to the inorganic-only parameterizations (Chang et al., 2016). No previous field studies have implemented the full resistor framework, but in this comparison, it was found to have worse agreement with WINTER results (higher median difference, higher RMSE, and lower  $r^2$ ) relative to the modified framework, when excluding chloride and including a dependence on O:C and RH. Agreement between the box model results and each organic parameterization remained the same or was slightly degraded (higher RMSE/lower  $r^2$ ) when particle  $\text{Cl}^-$  was included in the BT09 parameterization (Figures S28b–S28d and 14), suggesting that the magnitude of  $\text{Cl}^-$  enhancement may not apply to ambient aerosol. Overall, of the combined inorganic and organic parameterizations tested, the modified resistor method, mediated by the O:C ratio and RH, without a chloride enhancement (Figure 13i), best reproduced the WINTER  $\gamma(\text{N}_2\text{O}_5)$  values.

Considering all 14 parameterizations tested here, nine reproduced the median WINTER  $\gamma(\text{N}_2\text{O}_5)$ , within a factor of 2. Parameterizations with the worst agreement (largest RMSE and median percent difference) were the inorganic-only parameterizations most frequently used in chemical transport models, EJ05, Dav08, and BT09. Those with the best agreement either excluded the chloride enhancement in BT09 or accounted for an organic suppression of  $\gamma(\text{N}_2\text{O}_5)$ , mediated by the aerosol O:C ratio and ambient RH. None of the 14 parameterizations, however, were able to reproduce the 4 orders of magnitude range observed during WINTER, with an underprediction of the highest values and a roughly 1–2 orders of magnitude overprediction of WINTER values  $< 1 \times 10^{-3}$ . Overprediction of low values suggests an additional suppressive effect not accounted for by the current treatments of organics, possibly due to changes in uptake resistance (i.e., bulk-phase solubility, diffusion, or accommodation) associated with a change in aerosol morphology (i.e., liquid organic coating) or phase.



As previously shown, uptake is largely controlled by liquid water availability (relative to nitrate) with values  $< 1 \times 10^{-3}$  only observed in previous laboratory studies on solid particles (e.g., Kane et al., 2001),  $\text{NaNO}_3$  (Hallquist et al., 2003), some pure organic liquids (Gross et al., 2009; McNeill et al., 2006), and biogenic SOA (Anttila et al., 2006; Escorcia et al., 2010; Folkers et al., 2003). WINTER values  $< 1 \times 10^{-3}$  were nearly exclusive to a single flight (RF10) near Atlanta, GA (Figure 3). Section S7 presents a discussion of these low values (Hagerman et al., 1997; Xu et al., 2015) and describes three methods used for parameterizing the factors that may lead to suppression on this flight based on current understanding from laboratory studies, including phase separation of the organic fraction (i.e., a liquid organic coating) (You et al., 2014), changes in viscosity (Shiraiwa et al., 2017), or the presence of a large biogenic influence (Hu et al., 2015; Ng et al., 2010). These parameterizations, based on certain AMS mass factors and liquid water content, do not explain the low values from RF10. Lack of direct particle morphology (i.e., organic coatings) or phase measurements, however, leaves open the possibility that these factors contributed to  $\gamma(\text{N}_2\text{O}_5)$  suppression on RF10. While some variables such as O:C ratio and RH are thought to be predictive of morphology or phase, current parameterizations for  $\gamma(\text{N}_2\text{O}_5)$  have largely been developed for uptake onto internal mixtures of aqueous particles and may require additional terms to account for morphology (i.e., organic coatings), phase (i.e., glassy aerosol), and mixing state, which should be considered in future analyses of  $\gamma(\text{N}_2\text{O}_5)$  on ambient aerosol.

### 4.3.3. Empirical Parameterization

In addition to comparison of literature parameterizations, we derive the first field-based, empirical parameterization for  $\gamma(\text{N}_2\text{O}_5)$  that uses the same variables as the laboratory parameterizations but that fits the proportionality constants to obtain the best representation of WINTER observations. This parameterization (E6, Figure 13k) implements the simplified resistor model approach that best reproduced the WINTER results in section 4.3.2 and produces the lowest RMSE (0.0157) of any literature parameterizations tested. As in section S6 and briefly here, this method fits the ratio of  $k_{R5}/k_{R4}$  ( $= 0.04$ ),  $k_{R3}$  as a linear function of water ( $= 2.14 \times 10^5 [\text{H}_2\text{O}]$ ), and  $\varepsilon$  as a linear combination of RH and O:C ratio ( $= 0.15 \cdot \text{O:C} + 0.0016 \cdot \text{RH}$ ) (details in Table S8). Following the approach of Bertram and Thornton (2009),  $c$  is the mean molecular speed of  $\text{N}_2\text{O}_5$  ( $\text{m s}^{-1}$ ),  $V$  ( $\text{m}^3 \text{m}^{-3}$ ) and  $SA$  ( $\text{m}^2 \text{m}^{-3}$ ) are the aerosol volume and surface area densities, respectively, and the  $\text{N}_2\text{O}_5$  Henry's law coefficient ( $K_H$ ) is taken to be 51 (Fried et al., 1994). Following Riemer et al. (2009),  $R$  is the ideal gas constant ( $\text{m}^3 \text{atm K}^{-1} \text{mol}^{-1}$ ),  $T$  is temperature (K), and  $R_p$  (m),  $R_c$  (m), and  $\ell$  (m) represent the total particle radius, aqueous core radius, and organic coating thickness, respectively (described in section S6). The solubility and diffusion of  $\text{N}_2\text{O}_5$  through the organic coating are represented by the aqueous Henry's law ( $5,000 \text{ mol m}^{-3} \text{atm}^{-1}$ ; Anttila et al., 2006) and liquid diffusion ( $1 \times 10^{-9} \text{ m}^2 \text{s}^{-1}$ ; Riemer et al., 2009) coefficients, scaled by  $\varepsilon$  ( $= 0.15 \cdot \text{O:C} + 0.0016 \cdot \text{RH}$ ). The fit of this parameterization to WINTER data produced a  $k_{R5}/k_{R4}$  ratio within a factor of 2 to those presented in Griffiths et al. (2009) (0.03) and Bertram and Thornton (2009) (0.06), and a value of  $k_{R3}$  (for the average WINTER aerosol water molarity of 20 M) within a factor of 1.2 of Griffiths et al. (2009) ( $5 \times 10^6 \text{ s}^{-1}$ ) and 4 of Bertram and Thornton (2009) ( $1.1 \times 10^6 \text{ s}^{-1}$ ). Restricting the fit to O:C ratios within 0.5 and 1 (range of higher correlation in Figure 12), resulted in worse agreement.

$$\frac{1}{\gamma} = \frac{1}{\frac{4}{c} \frac{V}{SA} K_H \cdot 2.14 \times 10^5 [\text{H}_2\text{O}(l)] \left( 1 - \frac{1}{\left( \frac{0.04 [\text{H}_2\text{O}(l)]}{[\text{NO}_3^-]} \right) + 1} \right)} + \frac{1}{\frac{4RT(0.15 \cdot \text{O:C} + 0.0016 \cdot \text{RH}) \cdot H_{\text{aq}} D_{\text{aq}} R_c}{c \ell R_p}} \quad (6)$$

Parameterization of  $\gamma(\text{N}_2\text{O}_5)$  as a function of temperature, RH, and aerosol water and composition, using a mechanistically accurate empirical fit, has the advantage of reproducing the median value from WINTER but, like other literature parameterizations, cannot reproduce the large-scale variability. The failure of this parameterization suggests that there may be other factors that determine  $\gamma(\text{N}_2\text{O}_5)$ , such as aerosol morphology (i.e., liquid organic coatings), mixing state, and/or phase. Measurements of these properties should be included in future measurements of  $\text{NO}_x$ ,  $\text{O}_3$ , and  $\text{N}_2\text{O}_5$  to test their relevance to understanding  $\text{N}_2\text{O}_5$  uptake in ambient air.

## 5. Summary and Conclusions

A box model analysis of nocturnal reactive nitrogen chemistry derived 2,876 individual  $\gamma(\text{N}_2\text{O}_5)$  values with a median of 0.0143 during periods of darkness on 9 flights over the eastern United States during the 6-week



WINTER campaign. In comparison to all previous field determinations of  $\gamma(\text{N}_2\text{O}_5)$ , this analysis produced the largest observed range ( $2 \times 10^{-5}$  to 0.1751) in  $\gamma(\text{N}_2\text{O}_5)$  with nearly 50 times more data points than all previous aircraft campaigns combined. Comparison to the steady state approximation and 18 sensitivity studies of model parameter uncertainties provided an assessment of the box model robustness. The campaign median  $\gamma(\text{N}_2\text{O}_5)$  value was most sensitive to uncertainties in the measured aerosol SA density, similar to all previous field-derived results. The box model results generally agreed with the steady state approximation for  $\gamma(\text{N}_2\text{O}_5)$  at long simulation durations. Compared to a previous modeling sensitivity study, all but the lowest 5% of WINTER  $\gamma(\text{N}_2\text{O}_5)$  occurred within the range of values where global burdens of tropospheric oxidants and  $\text{NO}_x$  are most sensitive to this parameter, highlighting the need for an accurate parameterization of  $\gamma(\text{N}_2\text{O}_5)$  for 3-D chemical transport models.

Further analysis of correlations between WINTER  $\gamma(\text{N}_2\text{O}_5)$  values and RH, temperature, and aerosol composition generally followed trends previously observed in laboratory studies and field campaigns (when trends were observed). These results support the current proposed mechanism for uptake and suggest that aerosol water is the dominant controlling factor of ambient  $\gamma(\text{N}_2\text{O}_5)$ , out of all those proposed and measured. Despite general agreement with past studies, low correlation coefficients with all observed variables suggest that  $\gamma(\text{N}_2\text{O}_5)$  is either simultaneously dependent on multiple factors or is at least partly dependent on variables not captured in the ambient WINTER observations. Infrequently measured parameters known to influence  $\gamma(\text{N}_2\text{O}_5)$  include aerosol organic coatings and/or phase state. This analysis was also the first to quantitatively assess the dependence of field-derived  $\gamma(\text{N}_2\text{O}_5)$  on aerosol pH but found no evidence in the WINTER data that an acid-catalyzed mechanism is an important factor in  $\text{N}_2\text{O}_5$  uptake efficiency.

Finally, application of 14 literature parameterizations to WINTER data showed that predictions of  $\gamma(\text{N}_2\text{O}_5)$  based on pure inorganic and mixed aerosol components (assuming an organic suppression by either reactively thin or thick coatings or by reduction in mass accommodation) generally reproduced the WINTER median but with a 1–2 orders of magnitude underprediction in the observed range. In four parameterizations, agreement improved when the effect of chloride enhancement was excluded. Best agreement was observed with the simplified resistor model framework, which was further fit to WINTER observations to derive the first field-based, empirical parameterization of  $\gamma(\text{N}_2\text{O}_5)$ . Gross overprediction by all parameterizations, however, of lowest WINTER values  $< 1 \times 10^{-3}$  suggests an additional suppressive effect not captured by observed variables or parameterization framework. In the absence of measured organic composition data, the cause of low WINTER values could not be confirmed, but comparisons to previous laboratory studies suggest that aerosol morphology or phase-relevant variables may be stronger predictors of  $\gamma(\text{N}_2\text{O}_5)$  than those measured during WINTER and currently included in  $\gamma(\text{N}_2\text{O}_5)$  parameterizations. While factors such as aerosol water and nitrate appear to be important predictors of  $\gamma(\text{N}_2\text{O}_5)$ , measurements of aerosol organic composition and phase should, therefore, be considered in future field campaigns aimed at understanding the mechanism of heterogeneous  $\text{N}_2\text{O}_5$  uptake and its impacts on tropospheric oxidant distributions.

#### Acknowledgments

The authors would like to thank the NSF-NCAR Research Aircraft Facility staff. E. E. M. and S. S. B. acknowledge support from the NOAA Atmospheric Chemistry, Climate and Carbon Cycle (AC4) Program. Funding for D. L. F. was supported by NSF award 1433358. J. A. T., F. L. -H., and B. H. L. were supported by NSF award AGS-1360745. J. C. S., P. C. J., and J. L. J. were supported by NSF AGS-1360834 and US EPA 83587701-0. This paper has not been formally reviewed by EPA. The views expressed in this document are solely those of the authors and do not necessarily reflect those of EPA. EPA does not endorse any products or commercial services mentioned in this publication. All data from the WINTER campaign are available at [http://data.eol.ucar.edu/master\\_list/?project=WINTER](http://data.eol.ucar.edu/master_list/?project=WINTER). All referenced supplemental text, figures, and tables can be found in the supporting information. Code for the iterative box model can be found at <https://esrl.noaa.gov/csd/groups/csd7/measurements/2015winter/pubs/>.

#### References

- Aldener, M., Brown, S. S., Stark, H., Williams, E. J., Lerner, B. M., Kuster, W. C., et al. (2006). Reactivity and loss mechanisms of  $\text{NO}_3$  and  $\text{N}_2\text{O}_5$  in a polluted marine environment: Results from in situ measurements during New England air quality study 2002. *Journal of Geophysical Research*, 111, D23S73. <https://doi.org/10.1029/2006JD007252>
- Anttila, T., Kiendler-Scharr, A., Tillmann, R., & Mentel, T. F. (2006). On the reactive uptake of gaseous compounds by organic-coated aqueous aerosols: Theoretical analysis and application to the heterogeneous hydrolysis of  $\text{N}_2\text{O}_5$ . *The Journal of Physical Chemistry A*, 110(35), 10435–10443. <https://doi.org/10.1021/jp062403c>
- Apel, E. C., Hornbrook, R. S., Hills, A. J., Blake, N. J., Barth, M. C., Weinheimer, A., et al. (2015). Upper tropospheric ozone production from lightning  $\text{NO}_x$ -impacted convection: Smoke ingestion case study from the DC3 campaign. *Journal of Geophysical Research: Atmospheres*, 120, 2505–2523. <https://doi.org/10.1002/2014JD022121>
- Apodaca, R. L., Huff, D. M., & Simpson, W. R. (2008). The role of ice in  $\text{N}_2\text{O}_5$  heterogeneous hydrolysis at high latitudes. *Atmospheric Chemistry and Physics*, 8(24), 7451–7463. <https://doi.org/10.5194/acp-8-7451-2008>
- Atkinson, R., & Arey, J. (2003). Atmospheric degradation of volatile organic compounds. *Chemical Reviews*, 103(12), 4605–4638. <https://doi.org/10.1021/cr0206420>
- Attwood, A. R., Washenfelder, R. A., Brock, C. A., Hu, W., Baumann, K., Campuzano-Jost, P., et al. (2014). Trends in sulfate and organic aerosol mass in the southeast U.S.: Impact on aerosol optical depth and radiative forcing. *Geophysical Research Letters*, 41, 7701–7709. <https://doi.org/10.1002/2014GL061669>
- Baasandorj, M., Hoch, S. W., Bares, R., Lin, J. C., Brown, S. S., Millet, D. B., et al. (2017). Coupling between chemical and meteorological processes under persistent cold-air pool conditions: Evolution of wintertime  $\text{PM}_{2.5}$  pollution events and  $\text{N}_2\text{O}_5$  observations in Utah's Salt Lake Valley. *Environmental Science & Technology*, 51(11), 5941–5950. <https://doi.org/10.1021/acs.est.6b06603>

- Badger, C. L., Griffiths, P. T., George, I., Abbatt, J. P. D., & Cox, R. A. (2006). Reactive uptake of  $\text{N}_2\text{O}_5$  by aerosol particles containing mixtures of humic acid and ammonium sulfate. *The Journal of Physical Chemistry A*, 110(21), 6986–6994. <https://doi.org/10.1021/jp0562678>
- Behnke, W., George, C., Scheer, V., & Zetzsch, C. (1997). Production and decay of  $\text{ClNO}_2$  from the reaction of gaseous  $\text{N}_2\text{O}_5$  with NaCl solution: Bulk and aerosol experiments. *Journal of Geophysical Research*, 102, 3795–3804. <https://doi.org/10.1029/96JD03057>
- Behnke, W., Krüger, H. U., Scheer, V., & Zetzsch, C. (1991). Formation of atomic Cl from sea spray via photolysis of nitryl chloride: Determination of the sticking coefficient of  $\text{N}_2\text{O}_5$  on NaCl aerosol. *Journal of Aerosol Science*, 22, S609–S612. [https://doi.org/10.1016/S0021-8502\(05\)80175-2](https://doi.org/10.1016/S0021-8502(05)80175-2)
- Bertram, A. K., Martin, S. T., Hanna, S. J., Smith, M. L., Bodsworth, A., Chen, Q., et al. (2011). Predicting the relative humidities of liquid-liquid phase separation, efflorescence, and deliquescence of mixed particles of ammonium sulfate, organic material, and water using the organic-to-sulfate mass ratio of the particle and the oxygen-to-carbon elemental ratio of the organic component. *Atmospheric Chemistry and Physics*, 11(21), 10,995–11,006. <https://doi.org/10.5194/acp-11-10995-2011>
- Bertram, T. H., & Thornton, J. A. (2009). Toward a general parameterization of  $\text{N}_2\text{O}_5$  reactivity on aqueous particles: The competing effects of particle liquid water, nitrate and chloride. *Atmospheric Chemistry and Physics*, 9(21), 8351–8363. <https://doi.org/10.5194/acp-9-8351-2009>
- Bertram, T. H., Thornton, J. A., & Riedel, T. P. (2009). An experimental technique for the direct measurement of  $\text{N}_2\text{O}_5$  reactivity on ambient particles. *Atmospheric Measurement Techniques*, 2(1), 231–242. <https://doi.org/10.5194/amt-2-231-2009>
- Bertram, T. H., Thornton, J. A., Riedel, T. P., Middlebrook, A. M., Bahreini, R., Bates, T. S., et al. (2009). Direct observations of  $\text{N}_2\text{O}_5$  reactivity on ambient aerosol particles. *Geophysical Research Letters*, 36, L19803. <https://doi.org/10.1029/2009GL040248>
- Brock, C. A., Wagner, N. L., Anderson, B. E., Attwood, A. R., Beyersdorf, A., Campuzano-Jost, P., et al. (2016). Aerosol optical properties in the southeastern United States in summer—Part 1: Hygroscopic growth. *Atmospheric Chemistry and Physics*, 16(8), 4987–5007. <https://doi.org/10.5194/acp-16-4987-2016>
- Brown, S. S., Dubé, W. P., Fuchs, H., Ryerson, T. B., Wollny, A. G., Brock, C. A., et al. (2009). Reactive uptake coefficients for  $\text{N}_2\text{O}_5$  determined from aircraft measurements during the Second Texas Air Quality Study: Comparison to current model parameterizations. *Journal of Geophysical Research*, 114, D00F10. <https://doi.org/10.1029/2008JD011679>
- Brown, S. S., Dubé, W. P., Tham, Y. J., Zha, Q., Xue, L., Poon, S., et al. (2016). Nighttime chemistry at a high altitude site above Hong Kong. *Journal of Geophysical Research: Atmospheres*, 121, 2457–2475. <https://doi.org/10.1002/2015JD024566>
- Brown, S. S., Osthoff, H. D., Stark, H., Dubé, W. P., Ryerson, T. B., Warneke, C., et al. (2005). Aircraft observations of daytime  $\text{NO}_3$  and  $\text{N}_2\text{O}_5$  and their implications for tropospheric chemistry. *Journal of Photochemistry and Photobiology A: Chemistry*, 176(1–3), 270–278. <https://doi.org/10.1016/j.jphotochem.2005.10.004>
- Brown, S. S., Ryerson, T. B., Wollny, A. G., Brock, C. A., Peltier, R., Sullivan, A. P., et al. (2006). Variability in nocturnal nitrogen oxide processing and its role in regional air quality. *Science*, 311(5757), 67–70. <https://doi.org/10.1126/science.1120120>
- Brown, S. S., Stark, H., & Ravishankara, A. R. (2003). Applicability of the steady state approximation to the interpretation of atmospheric observations of  $\text{NO}_3$  and  $\text{N}_2\text{O}_5$ . *Journal of Geophysical Research*, 108(D17), 4539. <https://doi.org/10.1029/2003JD003407>
- Brown, S. S., & Stutz, J. (2012). Nighttime radical observations and chemistry. *Chemical Society Reviews*, 41(19), 6405–6447. <https://doi.org/10.1039/c2cs35181a>
- Cai, Y., Montague, D. C., Mooiweer-Bryan, W., & Deshler, T. (2008). Performance characteristics of the ultra high sensitivity aerosol spectrometer for particles between 55 and 800 nm: Laboratory and field studies. *Journal of Aerosol Science*, 39(9), 759–769. <https://doi.org/10.1016/j.jaerosci.2008.04.007>
- Cerully, K. M., Bougiatioti, A., Hite, J. R. Jr., Guo, H., Xu, L., Ng, N. L., et al. (2015). On the link between hygroscopicity, volatility, and oxidation state of ambient and water-soluble aerosols in the southeastern United States. *Atmospheric Chemistry and Physics*, 15(15), 8679–8694. <https://doi.org/10.5194/acp-15-8679-2015>
- Chang, R. Y. W., Slowik, J. G., Shantz, N. C., Vlasenko, A., Liggio, J., Sjostedt, S. J., et al. (2010). The hygroscopicity parameter ( $\kappa$ ) of ambient organic aerosol at a field site subject to biogenic and anthropogenic influences: Relationship to degree of aerosol oxidation. *Atmospheric Chemistry and Physics*, 10(11), 5047–5064. <https://doi.org/10.5194/acp-10-5047-2010>
- Chang, W. L., Bhawe, P. V., Brown, S. S., Riemer, N., Stutz, J., & Dabdub, D. (2011). Heterogeneous atmospheric chemistry, ambient measurements, and model calculations of  $\text{N}_2\text{O}_5$ : A review. *Aerosol Science and Technology*, 45(6), 665–695. <https://doi.org/10.1080/02786826.2010.551672>
- Chang, W. L., Brown, S. S., Stutz, J., Middlebrook, A. M., Bahreini, R., Wagner, N. L., et al. (2016). Evaluating  $\text{N}_2\text{O}_5$  heterogeneous hydrolysis parameterizations for CalNex 2010. *Journal of Geophysical Research: Atmospheres*, 121, 5051–5070. <https://doi.org/10.1002/2015JD024737>
- Cosman, L. M., Knopf, D. A., & Bertram, A. K. (2008).  $\text{N}_2\text{O}_5$  reactive uptake on aqueous sulfuric acid solutions coated with branched and straight-chain insoluble organic surfactants. *Journal of Physical Chemistry A*, 112(11), 2386–2396. <https://doi.org/10.1021/jp710685r>
- Davidovits, P., Kolb, C. E., Williams, L. R., Jayne, J. T., & Worsnop, D. R. (2006). Mass accommodation and chemical reactions at gas–liquid interfaces. *Chemical Reviews*, 106(4), 1323–1354. <https://doi.org/10.1021/cr040366k>
- Davis, J. M., Bhawe, P. V., & Foley, K. M. (2008). Parameterization of  $\text{N}_2\text{O}_5$  reaction probabilities on the surface of particles containing ammonium, sulfate, and nitrate. *Atmospheric Chemistry and Physics*, 8(17), 5295–5311. <https://doi.org/10.5194/acp-8-5295-2008>
- Day, D. A., Wooldridge, P. J., Dillon, M. B., Thornton, J. A., & Cohen, R. C. (2002). A thermal dissociation laser-induced fluorescence instrument for in situ detection of  $\text{NO}_2$ , peroxy nitrates, alkyl nitrates, and  $\text{HNO}_3$ . *Journal of Geophysical Research*, 107(D6), 4046. <https://doi.org/10.1029/2001JD000779>
- DeCarlo, P. F., Kimmel, J. R., Trimborn, A., Northway, M. J., Jayne, J. T., Aiken, A. C., et al. (2006). Field-deployable, high-resolution, time-of-flight aerosol mass spectrometer. *Analytical Chemistry*, 78(24), 8281–8289. <https://doi.org/10.1021/ac061249n>
- Dentener, F. J., & Crutzen, P. J. (1993). Reaction of  $\text{N}_2\text{O}_5$  on tropospheric aerosols: Impact on the global distributions of  $\text{NO}_x$ ,  $\text{O}_3$ , and OH. *Journal of Geophysical Research*, 98, 7149–7163. <https://doi.org/10.1029/92jd02979>
- Dockery, D. W., Pope, C. A., Xu, X., Spengler, J. D., Ware, J. H., Fay, M. E., et al. (1993). An association between air pollution and mortality in six U.S. cities. *New England Journal of Medicine*, 329(24), 1753–1759. <https://doi.org/10.1056/NEJM199312093292401>
- Dubé, W. P., Brown, S. S., Osthoff, H. D., Nunley, M. R., Ciciora, S. J., Paris, M. W., et al. (2006). Aircraft instrument for simultaneous, in situ measurement of  $\text{NO}_3$  and  $\text{N}_2\text{O}_5$  via pulsed cavity ring-down spectroscopy. *Review of Scientific Instruments*, 77(3), 034101. <https://doi.org/10.1063/1.2176058>
- Escorcia, E. N., Sjostedt, S. J., & Abbatt, J. P. D. (2010). Kinetics of  $\text{N}_2\text{O}_5$  hydrolysis on secondary organic aerosol and mixed ammonium bisulfate—secondary organic aerosol particles. *Journal of Physical Chemistry A*, 114(50), 13,113–13,121. <https://doi.org/10.1021/jp107721v>
- Evans, M. J., & Jacob, D. J. (2005). Impact of new laboratory studies of  $\text{N}_2\text{O}_5$  hydrolysis on global model budgets of tropospheric nitrogen oxides, ozone, and OH. *Geophysical Research Letters*, 32, L09813. <https://doi.org/10.1029/2005GL022469>
- Folkers, M. (2001). Bestimmung der Reaktionswahrscheinlichkeit von  $\text{N}_2\text{O}_5$  an troposphärisch relevanten Aerosolen (PhD thesis.) Universität Köln.

- Folkers, M., Mentel, T. F., & Wahner, A. (2003). Influence of an organic coating on the reactivity of aqueous aerosols probed by the heterogeneous hydrolysis of  $\text{N}_2\text{O}_5$ . *Geophysical Research Letters*, 30(12), 1644. <https://doi.org/10.1029/2003GL017168>
- Fountoukis, C., & Nenes, A. (2007). ISORROPIA II: A computationally efficient thermodynamic equilibrium model for  $\text{K}^+$ - $\text{Ca}^{2+}$ - $\text{Mg}^{2+}$ - $\text{NH}_4^+$ - $\text{Na}^+$ - $\text{SO}_4^{2-}$ - $\text{NO}_3^-$ - $\text{Cl}^-$ - $\text{H}_2\text{O}$  aerosols. *Atmospheric Chemistry and Physics*, 7(17), 4639–4659. <https://doi.org/10.5194/acp-7-4639-2007>
- Fried, A., Henry, B. E., Calvert, J. G., & Mozurkewich, M. (1994). The reaction probability of  $\text{N}_2\text{O}_5$  with sulfuric acid aerosols at stratospheric temperatures and compositions. *Journal of Geophysical Research*, 99, 3517–3532. <https://doi.org/10.1029/93JD01907>
- Fuchs, H., Dube, W. P., Cicioira, S. J., & Brown, S. S. (2008). Determination of inlet transmission and conversion efficiencies for in situ measurements of the nocturnal nitrogen oxides,  $\text{NO}_3$ ,  $\text{N}_2\text{O}_5$  and  $\text{NO}_2$ , via pulsed cavity ring-down spectroscopy. *Analytical Chemistry*, 80(15), 6010–6017. <https://doi.org/10.1021/Ac8007253>
- Fuchs, H., Dube, W. P., Lerner, B. M., Wagner, N. L., Williams, E. J., & Brown, S. S. (2009). A sensitive and versatile detector for atmospheric  $\text{NO}_2$  and  $\text{NO}_x$  based on blue diode laser cavity ring-down spectroscopy. *Environmental Science & Technology*, 43(20), 7831–7836. <https://doi.org/10.1021/es902067h>
- Fuchs, H., & Sutugin, A. G. (1970). *Highly dispersed aerosols*. Ann Arbor MI: Ann Arbor Science.
- Gaston, C. J., & Thornton, J. A. (2016). Reacto-diffusive length of  $\text{N}_2\text{O}_5$  in aqueous sulfate- and chloride-containing aerosol particles. *Journal of Physical Chemistry A*, 120(7), 1039–1045. <https://doi.org/10.1021/acs.jpca.5b11914>
- Gaston, C. J., Thornton, J. A., & Ng, N. L. (2014). Reactive uptake of  $\text{N}_2\text{O}_5$  to internally mixed inorganic and organic particles: The role of organic carbon oxidation state and inferred organic phase separations. *Atmospheric Chemistry and Physics*, 14(11), 5693–5707. <https://doi.org/10.5194/acp-14-5693-2014>
- George, C., Ponche, J. L., Mirabel, P., Behnke, W., Scheer, V., & Zetzsch, C. (1994). Study of the uptake of  $\text{N}_2\text{O}_5$  by water and NaCl solutions. *The Journal of Physical Chemistry*, 98(35), 8780–8784. <https://doi.org/10.1021/j100086a031>
- Griffiths, P. T., Badger, C. L., Cox, R. A., Folkers, M., Henk, H. H., & Mentel, T. F. (2009). Reactive uptake of  $\text{N}_2\text{O}_5$  by aerosols containing dicarboxylic acids. Effect of particle phase, composition, and nitrate content. *The Journal of Physical Chemistry A*, 113(17), 5082–5090. <https://doi.org/10.1021/jp8096814>
- Griffiths, P. T., & Cox, A. R. (2009). Temperature dependence of heterogeneous uptake of  $\text{N}_2\text{O}_5$  by ammonium sulfate aerosol. *Atmospheric Science Letters*, 10(3), 159–163. <https://doi.org/10.1002/asl.225>
- Gross, S., Iannone, R., Xiao, S., & Bertram, A. K. (2009). Reactive uptake studies of  $\text{NO}_3$  and  $\text{N}_2\text{O}_5$  on alkenoic acid, alkanoate, and polyalcohol substrates to probe nighttime aerosol chemistry. *Physical Chemistry Chemical Physics*, 11(36), 7792–7803. <https://doi.org/10.1039/B904741G>
- Guo, H., Sullivan, A. P., Campuzano-Jost, P., Schroder, J. C., Lopez-Hilfiker, F. D., Dibb, J. E., et al. (2016). Fine particle pH and the partitioning of nitric acid during winter in the northeastern United States. *Journal of Geophysical Research: Atmospheres*, 121, 10,355–10,376. <https://doi.org/10.1002/2016JD025311>
- Hagerman, L. M., Aneja, V. P., & Lonneman, W. A. (1997). Characterization of non-methane hydrocarbons in the rural southeast United States. *Atmospheric Environment*, 31(23), 4017–4038. [https://doi.org/10.1016/S1352-2310\(97\)00223-9](https://doi.org/10.1016/S1352-2310(97)00223-9)
- Hallquist, M., Stewart, D. J., Baker, J., & Cox, R. A. (2000). Hydrolysis of  $\text{N}_2\text{O}_5$  on submicron sulfuric acid aerosols. *The Journal of Physical Chemistry A*, 104(17), 3984–3990. <https://doi.org/10.1021/jp9939625>
- Hallquist, M., Stewart, D. J., Stephenson, S. K., & Anthony Cox, R. (2003). Hydrolysis of  $\text{N}_2\text{O}_5$  on sub-micron sulfate aerosols. *Physical Chemistry Chemical Physics*, 5(16), 3453–3463. <https://doi.org/10.1039/B301827J>
- Hjorth, J., Ottobri, G., & Restelli, G. (1986). Reaction of the  $\text{NO}_3$  radical with CO: Determination of an upper limit for the rate constant using FTIR spectroscopy. *International Journal of Chemical Kinetics*, 18(8), 819–827. <https://doi.org/10.1002/kin.550180802>
- Hodzic, A., & Jimenez, J. L. (2011). Modeling anthropogenically controlled secondary organic aerosols in a megacity: A simplified framework for global and climate models. *Geoscientific Model Development*, 4(4), 901–917. <https://doi.org/10.5194/gmd-4-901-2011>
- Hu, J. H., & Abbatt, J. P. D. (1997). Reaction probabilities for  $\text{N}_2\text{O}_5$  hydrolysis on sulfuric acid and ammonium sulfate aerosols at room temperature. *The Journal of Physical Chemistry A*, 101(5), 871–878. <https://doi.org/10.1021/jp9627436>
- Hu, W. W., Campuzano-Jost, P., Palm, B. B., Day, D. A., Ortega, A. M., Hayes, P. L., et al. (2015). Characterization of a real-time tracer for isoprene epoxydiols-derived secondary organic aerosol (IEPOX-SOA) from aerosol mass spectrometer measurements. *Atmospheric Chemistry and Physics*, 15(20), 11,807–11,833. <https://doi.org/10.5194/acp-15-11807-2015>
- IUPAC (2008). Data sheet  $\text{NO}_3$ . Retrieved from <http://iupac.pole-ether.fr>
- Jimenez, J. L., Canagaratna, M. R., Donahue, N. M., Prevot, A. S. H., Zhang, Q., Kroll, J. H., et al. (2009). Evolution of organic aerosols in the atmosphere. *Science*, 326(5959), 1525–1529. <https://doi.org/10.1126/science.1180353>
- Kane, S. M., Caloz, F., & Leu, M.-T. (2001). Heterogeneous uptake of gaseous  $\text{N}_2\text{O}_5$  by  $(\text{NH}_4)_2\text{SO}_4$ ,  $\text{NH}_4\text{HSO}_4$ , and  $\text{H}_2\text{SO}_4$  aerosols. *The Journal of Physical Chemistry A*, 105(26), 6465–6470. <https://doi.org/10.1021/jp010490x>
- Kim, M. J., Farmer, D. K., & Bertram, T. H. (2014). A controlling role for the air–sea interface in the chemical processing of reactive nitrogen in the coastal marine boundary layer. *Proceedings of the National Academy of Sciences of the United States of America*, 111(11), 3943–3948. <https://doi.org/10.1073/pnas.1318694111>
- Kim, P. S., Jacob, D. J., Fisher, J. A., Travis, K., Yu, K., Zhu, L., et al. (2015). Sources, seasonality, and trends of southeast US aerosol: An integrated analysis of surface, aircraft, and satellite observations with the GEOS-Chem chemical transport model. *Atmospheric Chemistry and Physics*, 15(18), 10,411–10,433. <https://doi.org/10.5194/acp-15-10411-2015>
- Kolb, C. E., Davidovits, P., Jayne, J. T., Shi, Q., & Worsnop, D. R. (2002). Kinetics of trace gas uptake by liquid surfaces. *Progress in Reaction Kinetics and Mechanism*, 27(1), 1–46. <https://doi.org/10.3184/007967402103165324>
- Lee, B. H., Lopez-Hilfiker, F. D., Mohr, C., Kurtén, T., Worsnop, D. R., & Thornton, J. A. (2014). An iodide-adduct high-resolution time-of-flight chemical-ionization mass spectrometer: Application to atmospheric inorganic and organic compounds. *Environmental Science & Technology*, 48(11), 6309–6317. <https://doi.org/10.1021/es500362a>
- Losey, D. J., Parker, R. G., & Freedman, M. A. (2016). pH dependence of liquid–liquid phase separation in organic aerosol. *The Journal of Physical Chemistry Letters*, 7(19), 3861–3865. <https://doi.org/10.1021/acs.jpclett.6b01621>
- Macintyre, H. L., & Evans, M. J. (2010). Sensitivity of a global model to the uptake of  $\text{N}_2\text{O}_5$  by tropospheric aerosol. *Atmospheric Chemistry and Physics*, 10(15), 7409–7414. <https://doi.org/10.5194/acp-10-7409-2010>
- Mao, J., Paulot, F., Jacob, D. J., Cohen, R. C., Crounse, J. D., Wennberg, P. O., et al. (2013). Ozone and organic nitrates over the eastern United States: Sensitivity to isoprene chemistry. *Journal of Geophysical Research: Atmospheres*, 118, 11,256–11,268. <https://doi.org/10.1002/jgrd.50817>
- McNeill, V. F., Patterson, J., Wolfe, G. M., & Thornton, J. A. (2006). The effect of varying levels of surfactant on the reactive uptake of  $\text{N}_2\text{O}_5$  to aqueous aerosol. *Atmospheric Chemistry and Physics*, 6(6), 1635–1644. <https://doi.org/10.5194/acp-6-1635-2006>

- Mei, F., Hayes, P. L., Ortega, A., Taylor, J. W., Allan, J. D., Gilman, J., et al. (2013). Droplet activation properties of organic aerosols observed at an urban site during CalNex-LA. *Journal of Geophysical Research: Atmospheres*, 118, 2903–2917. <https://doi.org/10.1002/jgrd.50285>
- Mentel, T. F., Bleilebens, D., & Wahner, A. (1996). A study of nighttime nitrogen oxide oxidation in a large reaction chamber—The fate of NO<sub>2</sub>, N<sub>2</sub>O<sub>5</sub>, HNO<sub>3</sub>, and O<sub>3</sub> at different humidities. *Atmospheric Environment*, 30(23), 4007–4020. [https://doi.org/10.1016/1352-2310\(96\)00117-3](https://doi.org/10.1016/1352-2310(96)00117-3)
- Mentel, T. F., Sohn, M., & Wahner, A. (1999). Nitrate effect in the heterogeneous hydrolysis of dinitrogen pentoxide on aqueous aerosols. *Physical Chemistry Chemical Physics*, 1(24), 5451–5457. <https://doi.org/10.1039/A905338G>
- Morgan, W. T., Ouyang, B., Allan, J. D., Aruffo, E., Di Carlo, P., Kennedy, O. J., et al. (2015). Influence of aerosol chemical composition on N<sub>2</sub>O<sub>5</sub> uptake: Airborne regional measurements in northwestern Europe. *Atmospheric Chemistry and Physics*, 15(2), 973–990. <https://doi.org/10.5194/acp-15-973-2015>
- Mozurkewich, M., & Calvert, J. G. (1988). Reaction probability of N<sub>2</sub>O<sub>5</sub> on aqueous aerosols. *Journal of Geophysical Research*, 93, 15,889–15,896. <https://doi.org/10.1029/JD093iD12p15889>
- Ng, N. L., Brown, S. S., Archibald, A. T., Atlas, E., Cohen, R. C., Crowley, J. N., et al. (2017). Nitrate radicals and biogenic volatile organic compounds: Oxidation, mechanisms, and organic aerosol. *Atmospheric Chemistry and Physics*, 17(3), 2103–2162. <https://doi.org/10.5194/acp-17-2103-2017>
- Ng, N. L., Canagaratna, M. R., Zhang, Q., Jimenez, J. L., Tian, J., Ulbrich, I. M., et al. (2010). Organic aerosol components observed in Northern Hemispheric datasets from aerosol mass spectrometry. *Atmospheric Chemistry and Physics*, 10(10), 4625–4641. <https://doi.org/10.5194/acp-10-4625-2010>
- Osthoff, H. D., Roberts, J. M., Ravishankara, A. R., Williams, E. J., Lerner, B. M., Sommariva, R., et al. (2008). High levels of nitryl chloride in the polluted subtropical marine boundary layer. *Nature Geoscience*, 1(5), 324–328. <https://doi.org/10.1038/ngeo177>
- Petters, M. D., & Kreidenweis, S. M. (2007). A single parameter representation of hygroscopic growth and cloud condensation nucleus activity. *Atmospheric Chemistry and Physics*, 7(8), 1961–1971. <https://doi.org/10.5194/acp-7-1961-2007>
- Phillips, G. J., Thieser, J., Tang, M., Sobanski, N., Schuster, G., Fachinger, J., et al. (2016). Estimating N<sub>2</sub>O<sub>5</sub> uptake coefficients using ambient measurements of NO<sub>3</sub>, N<sub>2</sub>O<sub>5</sub>, ClNO<sub>2</sub> and particle-phase nitrate. *Atmospheric Chemistry and Physics*, 16(20), 13,231–13,249. <https://doi.org/10.5194/acp-16-13231-2016>
- Pöschl, U., Rudich, Y., & Ammann, M. (2007). Kinetic model framework for aerosol and cloud surface chemistry and gas-particle interactions: Part 1: General equations, parameters, and terminology. *Atmospheric Chemistry and Physics*, 7(23), 5989–6023. <https://doi.org/10.5194/acp-7-5989-2007>
- Pusede, S. E., Duffey, K. C., Shusterman, A. A., Saleh, A., Laughner, J. L., Wooldridge, P. J., et al. (2016). On the effectiveness of nitrogen oxide reductions as a control over ammonium nitrate aerosol. *Atmospheric Chemistry and Physics*, 16(4), 2575–2596. <https://doi.org/10.5194/acp-16-2575-2016>
- Pye, H. O. T., Liao, H., Wu, S., Mickley, L. J., Jacob, D. J., Henze, D. K., & Seinfeld, J. H. (2009). Effect of changes in climate and emissions on future sulfate-nitrate-ammonium aerosol levels in the United States. *Journal of Geophysical Research*, 114, D01205. <https://doi.org/10.1029/2008JD010701>
- Rickards, A. M. J., Miles, R. E. H., Davies, J. F., Marshall, F. H., & Reid, J. P. (2013). Measurements of the sensitivity of aerosol hygroscopicity and the  $\kappa$  parameter to the O/C ratio. *The Journal of Physical Chemistry A*, 117(51), 14,120–14,131. <https://doi.org/10.1021/jp407991n>
- Riedel, T. P., Bertram, T. H., Ryder, O. S., Liu, S., Day, D. A., Russell, L. M., et al. (2012). Direct N<sub>2</sub>O<sub>5</sub> reactivity measurements at a polluted coastal site. *Atmospheric Chemistry and Physics*, 12(6), 2959–2968. <https://doi.org/10.5194/acp-12-2959-2012>
- Riemer, N., Vogel, H., Vogel, B., Anttila, T., Kiendler-Scharr, A., & Mentel, T. F. (2009). Relative importance of organic coatings for the heterogeneous hydrolysis of N<sub>2</sub>O<sub>5</sub> during summer in Europe. *Journal of Geophysical Research*, 114, D17307. <https://doi.org/10.1029/2008JD011369>
- Riemer, N., Vogel, H., Vogel, B., Schell, B., Ackermann, I., Kessler, C., & Hass, H. (2003). Impact of the heterogeneous hydrolysis of N<sub>2</sub>O<sub>5</sub> on chemistry and nitrate aerosol formation in the lower troposphere under photochemical conditions. *Journal of Geophysical Research*, 108(D4), 4144. <https://doi.org/10.1029/2002JD002436>
- Robinson, G. N., Worsnop, D. R., Jayne, J. T., Kolb, C. E., & Davidovits, P. (1997). Heterogeneous uptake of ClONO<sub>2</sub> and N<sub>2</sub>O<sub>5</sub> by sulfuric acid solutions. *Journal of Geophysical Research: Atmospheres*, 102, 3583–3601. <https://doi.org/10.1029/96JD03457>
- Ryder, O. S., Ault, A. P., Cahill, J. F., Guasco, T. L., Riedel, T. P., Cuadra-Rodriguez, L. A., et al. (2014). On the role of particle inorganic mixing state in the reactive uptake of N<sub>2</sub>O<sub>5</sub> to ambient aerosol particles. *Environmental Science & Technology*, 48(3), 1618–1627. <https://doi.org/10.1021/es4042622>
- Sarwar, G., Simon, H., Xing, J., & Mathur, R. (2014). Importance of tropospheric ClONO<sub>2</sub> chemistry across the Northern Hemisphere. *Geophysical Research Letters*, 41, 4050–4058. <https://doi.org/10.1002/2014GL059962>
- Schweitzer, F., Mirabel, P., & George, C. (1998). Multiphase chemistry of N<sub>2</sub>O<sub>5</sub>, ClONO<sub>2</sub>, and BrNO<sub>2</sub>. *The Journal of Physical Chemistry A*, 102(22), 3942–3952. <https://doi.org/10.1021/jp980748s>
- Seidel, D. J., Zhang, Y., Beljaars, A., Golaz, J.-C., Jacobson, A. R., & Medeiros, B. (2012). Climatology of the planetary boundary layer over the continental United States and Europe. *Journal of Geophysical Research*, 117, D17106. <https://doi.org/10.1029/2012JD018143>
- Shaloski, M. A., Gord, J. R., Staudt, S., Quinn, S. L., Bertram, T. H., & Nathanson, G. M. (2017). Reactions of N<sub>2</sub>O<sub>5</sub> with salty and surfactant-coated glycerol: Interfacial conversion of Br<sup>−</sup> to Br<sub>2</sub> mediated by alkylammonium cations. *The Journal of Physical Chemistry A*, 121(19), 3708–3719. <https://doi.org/10.1021/acs.jpca.7b02040>
- Shetter, R. E., & Müller, M. (1999). Photolysis frequency measurements using actinic flux spectroradiometry during the PEM-Tropics mission: Instrumentation description and some results. *Journal of Geophysical Research*, 104, 5647–5661. <https://doi.org/10.1029/98JD01381>
- Shingler, T., Crosbie, E., Ortega, A., Shiraiwa, M., Zuend, A., Beyersdorf, A., et al. (2016). Airborne characterization of subsaturated aerosol hygroscopicity and dry refractive index from the surface to 6.5 km during the SEAC4RS campaign. *Journal of Geophysical Research: Atmospheres*, 121, 4188–4210. <https://doi.org/10.1002/2015JD024498>
- Shiraiwa, M., Li, Y., Tsimpidi, A. P., Karydis, V. A., Berkemeier, T., Pandis, S. N., et al. (2017). Global distribution of particle phase state in atmospheric secondary organic aerosols. *Nature Communications*, 8, 15002. <https://doi.org/10.1038/ncomms15002>
- Sickles, J. E., & Shadwick, D. S. (2007). Changes in air quality and atmospheric deposition in the eastern United States: 1990–2004. *Journal of Geophysical Research*, 112, D17301. <https://doi.org/10.1029/2006JD007843>
- Sohn, M. (1998). Heterogene Reaktionen von Stickoxiden an Aerosolpartikeln, Doktorarbeit, Philipps-Universität Marburg.
- Stewart, D. J., Griffiths, P. T., & Cox, R. A. (2004). Reactive uptake coefficients for heterogeneous reaction of N<sub>2</sub>O<sub>5</sub> with submicron aerosols of NaCl and natural sea salt. *Atmospheric Chemistry and Physics*, 4(5), 1381–1388. <https://doi.org/10.5194/acp-4-1381-2004>
- Stone, D., Evans, M. J., Walker, H., Ingham, T., Vaughan, S., Ouyang, B., et al. (2014). Radical chemistry at night: Comparisons between observed and modelled HO<sub>x</sub>, NO<sub>3</sub> and N<sub>2</sub>O<sub>5</sub> during the RONOCO project. *Atmospheric Chemistry and Physics*, 14(3), 1299–1321. <https://doi.org/10.5194/acp-14-1299-2014>



- Strapp, J. W., Leaitch, W. R., & Liu, P. S. K. (1992). Hydrated and dried aerosol-size-distribution measurements from the particle measuring systems FSSP-300 probe and the deiced PCASP-100X probe. *Journal of Atmospheric and Oceanic Technology*, 9(5), 548–555. [https://doi.org/10.1175/1520-0426\(1992\)009%3C0548:HADASD%3E2.0.CO;2](https://doi.org/10.1175/1520-0426(1992)009%3C0548:HADASD%3E2.0.CO;2)
- Stull, R. B. (1988). *An introduction to boundary layer meteorology*. Dordrecht, Netherlands: Kluwer Academic.
- Suda, S. R., Petters, M. D., Matsunaga, A., Sullivan, R. C., Ziemann, P. J., & Kreidenweis, S. M. (2012). Hygroscopicity frequency distributions of secondary organic aerosols. *Journal of Geophysical Research*, 117, D04207. <https://doi.org/10.1029/2011JD016823>
- Tham, Y. J., Wang, Z., Li, Q., Yun, H., Wang, W., Wang, X., et al. (2016). Significant concentrations of nitryl chloride sustained in the morning: Investigations of the causes and impacts on ozone production in a polluted region of northern China. *Atmospheric Chemistry and Physics*, 16(23), 14,959–14,977. <https://doi.org/10.5194/acp-16-14959-2016>
- Thornton, J. A., & Abbatt, J. P. D. (2005). N<sub>2</sub>O<sub>5</sub> reaction on submicron sea salt aerosol: Kinetics, products, and the effect of surface active organics. *The Journal of Physical Chemistry A*, 109(44), 10,004–10,012. <https://doi.org/10.1021/jp054183t>
- Thornton, J. A., Braban, C. F., & Abbatt, J. P. D. (2003). N<sub>2</sub>O<sub>5</sub> hydrolysis on sub-micron organic aerosols: The effect of relative humidity, particle phase, and particle size. *Physical Chemistry Chemical Physics*, 5(20), 4593–4603. <https://doi.org/10.1039/B307498F>
- Thornton, J. A., Kercher, J. P., Riedel, T. P., Wagner, N. L., Cozic, J., Holloway, J. S., et al. (2010). A large atomic chlorine source inferred from mid-continental reactive nitrogen chemistry. *Nature*, 464(7286), 271–274. <https://doi.org/10.1038/nature08905>
- Tie, X., Brasseur, G., Emmons, L., Horowitz, L., & Kinnison, D. (2001). Effects of aerosols on tropospheric oxidants: A global model study. *Journal of Geophysical Research*, 106, 22,931–22,964. <https://doi.org/10.1029/2001JD00206>
- Van Doren, J. M., Watson, L. R., Davidovits, P., Worsnop, D. R., Zahniser, M. S., & Kolb, C. E. (1990). Temperature dependence of the uptake coefficients of nitric acid, hydrochloric acid and nitrogen oxide (N<sub>2</sub>O<sub>5</sub>) by water droplets. *The Journal of Physical Chemistry*, 94(8), 3265–3269. <https://doi.org/10.1021/j100371a009>
- Vaughan, S., Canosa-Mas, C. E., Pfrang, C., Shallcross, D. E., Watson, L., & Wayne, R. P. (2006). Kinetic studies of reactions of the nitrate radical (NO<sub>3</sub>) with peroxy radicals (RO<sub>2</sub>): An indirect source of OH at night? *Physical Chemistry Chemical Physics*, 8(32), 3749–3760. <https://doi.org/10.1039/B605569A>
- Wagner, N. L., Dubé, W. P., Washenfelder, R. A., Young, C. J., Pollack, I. B., Ryerson, T. B., & Brown, S. S. (2011). Diode laser-based cavity ring-down instrument for NO<sub>3</sub>, N<sub>2</sub>O<sub>5</sub>, NO, NO<sub>2</sub> and O<sub>3</sub> from aircraft. *Atmospheric Measurement Techniques*, 4(6), 1227–1240. <https://doi.org/10.5194/amt-4-1227-2011>
- Wagner, N. L., Riedel, T. P., Young, C. J., Bahreini, R., Brock, C. A., Dubé, W. P., et al. (2013). N<sub>2</sub>O<sub>5</sub> uptake coefficients and nocturnal NO<sub>2</sub> removal rates determined from ambient wintertime measurements. *Journal of Geophysical Research: Atmospheres*, 118, 9331–9350. <https://doi.org/10.1002/jgrd.50653>
- Wahner, A., Mentel, T. F., & Sohn, M. (1998). Gas-phase reaction of N<sub>2</sub>O<sub>5</sub> with water vapor: Importance of heterogeneous hydrolysis of N<sub>2</sub>O<sub>5</sub> and surface desorption of HNO<sub>3</sub> in a large Teflon chamber. *Geophysical Research Letters*, 25, 2169–2172. <https://doi.org/10.1029/98GL51596>
- Wahner, A., Mentel, T. F., Sohn, M., & Stier, J. (1998). Heterogeneous reaction of N<sub>2</sub>O<sub>5</sub> on sodium nitrate aerosol. *Journal of Geophysical Research: Atmospheres*, 103, 31,103–31,112. <https://doi.org/10.1029/1998JD100022>
- Wang, H., Lu, K., Chen, X., Zhu, Q., Chen, Q., Guo, S., et al. (2017). High N<sub>2</sub>O<sub>5</sub> concentrations observed in urban Beijing: Implications of a large nitrate formation pathway. *Environmental Science & Technology Letters*, 4(10), 416–420. <https://doi.org/10.1021/acs.estlett.7b00341>
- Wang, X., Wang, H., Xue, L., Wang, T., Wang, L., Gu, R., et al. (2017). Observations of N<sub>2</sub>O<sub>5</sub> and ClNO<sub>2</sub> at a polluted urban surface site in North China: High N<sub>2</sub>O<sub>5</sub> uptake coefficients and low ClNO<sub>2</sub> product yields. *Atmospheric Environment*, 156, 125–134. <https://doi.org/10.1016/j.atmosenv.2017.02.035>
- Wang, Z., Wang, W., Tham, Y. J., Li, Q., Wang, H., Wen, L., et al. (2017). Fast heterogeneous N<sub>2</sub>O<sub>5</sub> uptake and ClNO<sub>2</sub> production in power plant and industrial plumes observed in the nocturnal residual layer over the North China Plain. *Atmospheric Chemistry and Physics*, 17(20), 12,361–12,378. <https://doi.org/10.5194/acp-17-12361-2017>
- Washenfelder, R. A., Wagner, N. L., Dube, W. P., & Brown, S. S. (2011). Measurement of atmospheric ozone by cavity ring-down spectroscopy. *Environmental Science & Technology*, 45(7), 2938–2944. <https://doi.org/10.1021/es103340u>
- Weinheimer, A. J., Walega, J. G., Ridley, B. A., Gary, B. L., Blake, D. R., Blake, N. J., et al. (1994). Meridional distributions of NO<sub>x</sub>, NO<sub>y</sub>, and other species in the lower stratosphere and upper troposphere during AASE II. *Geophysical Research Letters*, 21, 2583–2586. <https://doi.org/10.1029/94GL01897>
- Wexler, A. S., & Clegg, S. L. (2002). Atmospheric aerosol models for systems including the ions H<sup>+</sup>, NH<sub>4</sub><sup>+</sup>, Na<sup>+</sup>, SO<sub>4</sub><sup>2-</sup>, NO<sub>3</sub><sup>-</sup>, Cl<sup>-</sup>, Br<sup>-</sup>, and H<sub>2</sub>O. *Journal of Geophysical Research*, 107(D14), 2156. <https://doi.org/10.1029/2001JD000451>
- Wild, R. J., Edwards, P. M., Bates, T. S., Cohen, R. C., de Gouw, J. A., Dubé, W. P., et al. (2016). Reactive nitrogen partitioning and its relationship to winter ozone events in Utah. *Atmospheric Chemistry and Physics*, 16(2), 573–583. <https://doi.org/10.5194/acp-16-573-2016>
- Wild, R. J., Edwards, P. M., Dube, W. P., Baumann, K., Edgerton, E. S., Quinn, P. K., et al. (2014). A measurement of total reactive nitrogen, NO<sub>y</sub>, together with NO<sub>2</sub>, NO, and O<sub>3</sub> via cavity ring-down spectroscopy. *Environmental Science & Technology*, 48(16), 9609–9615. <https://doi.org/10.1021/es501896w>
- Xu, L., Suresh, S., Guo, H., Weber, R. J., & Ng, N. L. (2015). Aerosol characterization over the southeastern United States using high-resolution aerosol mass spectrometry: Spatial and seasonal variation of aerosol composition and sources with a focus on organic nitrates. *Atmospheric Chemistry and Physics*, 15(13), 7307–7336. <https://doi.org/10.5194/acp-15-7307-2015>
- You, Y., Smith, M. L., Song, M., Martin, S. T., & Bertram, A. K. (2014). Liquid–liquid phase separation in atmospherically relevant particles consisting of organic species and inorganic salts. *International Reviews in Physical Chemistry*, 33(1), 43–77. <https://doi.org/10.1080/0144235X.2014.890786>
- Zhang, Q., Jimenez, J. L., Canagaratna, M. R., Allan, J. D., Coe, H., Ulbrich, I., et al. (2007). Ubiquity and dominance of oxygenated species in organic aerosols in anthropogenically-influenced Northern Hemisphere midlatitudes. *Geophysical Research Letters*, 34, L13801. <https://doi.org/10.1029/2007GL029979>